



Petrology, structural setting, timing, and geochemistry of Cretaceous volcanic rocks in eastern Mongolia: Constraints on their tectonic origin



Batulzii Dash ^a, An Yin ^{b,*}, Neng Jiang ^c, Bayartsengel Tseveendorj ^a, Baofu Han ^d

^a Department of Geology, Mongolian University of Science and Technology, Ulaan Baatar 210646, Mongolia

^b Department of Earth and Space Sciences, University of California Los Angeles, CA 90095-1567, USA

^c Key Laboratory for Mineral Resources Research, Institute of Geology and Geophysics, Chinese Academy of Sciences, P.O. Box 9825, Beijing 100029, China

^d School of Earth and Space Sciences, Peking University, Beijing 10871, China

ARTICLE INFO

Article history:

Received 1 March 2013

Received in revised form 20 September 2013

Accepted 8 October 2013

Available online 24 October 2013

Handling Editor: M. Santosh

Keywords:

Mongolia
Mesozoic arc
Eastern Asia
Back-arc magmatism

ABSTRACT

Cretaceous volcanism occurred over a wide region of eastern Asia. Hypotheses for its development include intra-continental rifting, continental-arc magmatism, plume activities, and delamination of a previously thickened mantle lithosphere. One of the major obstacles in differentiating the above model is the lack of systematic studies of Cretaceous volcanic rocks in eastern Mongolia and far-east Russia. In this study, we address this issue by examining the timing and geochemistry of Cretaceous volcanic rocks in eastern Mongolia. Our ⁴⁰Ar/³⁹Ar dating of volcanic rocks together with the existing K–Ar ages of volcanic rocks indicate that Cretaceous volcanism in our study area occurred between 120 Ma and 104 Ma. Our field investigation and geochemical analysis reveal three types of volcanic rocks in the study area: (1) a bimodal series, (2) a shoshonite series, and (3) a basanite series. Geochemical analysis of the volcanic rocks indicates a highly heterogeneous source, which is characterized by a mixture of depleted, enriched and metasomatized mantle. At least three models may explain the timing, geochemistry, and regional tectonic setting of Cretaceous volcanism in eastern Mongolia: (1) partial delamination of a previously thickened mantle lithosphere generated by arc magmatism and collision tectonics, (2) back-arc extension and its related mantle upwelling due to rapid collapse of a flat subduction slab, and (3) mantle avalanche of a thick pile of cold subducted Paleo-Asian oceanic plates initially trapped at the 670-km endothermic phase transition triggered by westward Pacific subduction causing mixing of several mantle sources. Testing the above models require further studies on the spatial and temporal relationships between Cretaceous volcanism and structural history of NE Asia. In addition, a careful restoration of the position and history of past subducted slabs of the Paleo-Asian oceans may help differentiate the above competing models in the future.

© 2013 International Association for Gondwana Research. Published by Elsevier B.V. All rights reserved.

1. Introduction

A 2000-km Cretaceous volcanic belt extends from eastern Mongolia, through the Greater Xing'an Mountains of NE China, to far-east Russia (Zonenshain et al., 1990; Badarch et al., 2002; Fan et al., 2003; Wu et al., 2005a; Wang et al., 2006; J.H. Zhang et al., 2008; L.C. Zhang et al., 2008; Ying et al., 2010a,b; Zhang et al., 2010, 2011) (Fig. 1). This belt can also be traced southward to SE Asia along the eastern margin of Asia (T.-D. Li, 2000; X.H. Li, 2000; Wu et al., 2005a). The northern part of the Cretaceous volcanic zone was constructed over a Neoproterozoic to Early Mesozoic orogen variably named as the Central Asian Fold Belt (Zonenshain et al., 1990), Central Asian Accretionary Orogen (Sengör et al., 1993), Central Asian Orogenic Belt (Jahn, 2004), or Central Asian Orogenic System (Briggs et al., 2007, 2009) (Fig. 1).

As the orogen is neither linear (i.e., not a belt) nor involving purely accretionary process (Kröner et al., 2014), we follow the usage of Briggs et al. (2007, 2009) and refer the orogen as the Central Asian Orogenic System (CAOS). The CAOS extends for >4000 km from the Tian Shan of central Asia in the west to the Sea of Okhotsk in the east (Sengör et al., 1993; Şengör and Natal'in, 1996; Briggs et al., 2007; Windley et al., 2007; Kelty et al., 2008; Briggs et al., 2009; Xiao et al., 2010; Wang et al., 2011; Kröner et al., 2014).

In eastern Mongolia, the Cretaceous volcanic rocks occur over Paleozoic accretionary complexes and turbidites (Badarch et al., 2002) (Fig. 2). In NE China, the Cretaceous volcanic rocks occurred across several Proterozoic terranes with metamorphic basement (e.g., Wang et al., 2011; Zhang et al., 2012) (Fig. 1). The tectonic evolution of eastern Mongolia and NE China has involved Late Paleozoic to Early Mesozoic subduction and closure of the Paleo-Asia oceans (e.g., Şengör and Natal'in, 1996; Yin and Nie, 1996; Zhang et al., 2012), followed immediately by the initiation of westward subduction of the Pacific plate below eastern Asia (e.g., Meng and Zhou, 1996; Şengör and Natal'in, 1996; Maruyama et al., 1997; Taira, 2001).

* Corresponding author.

E-mail addresses: ulziid@yahoo.com (B. Dash), yin@ess.ucla.edu (A. Yin), jiangneng@mail.igcas.ac.cn (N. Jiang).

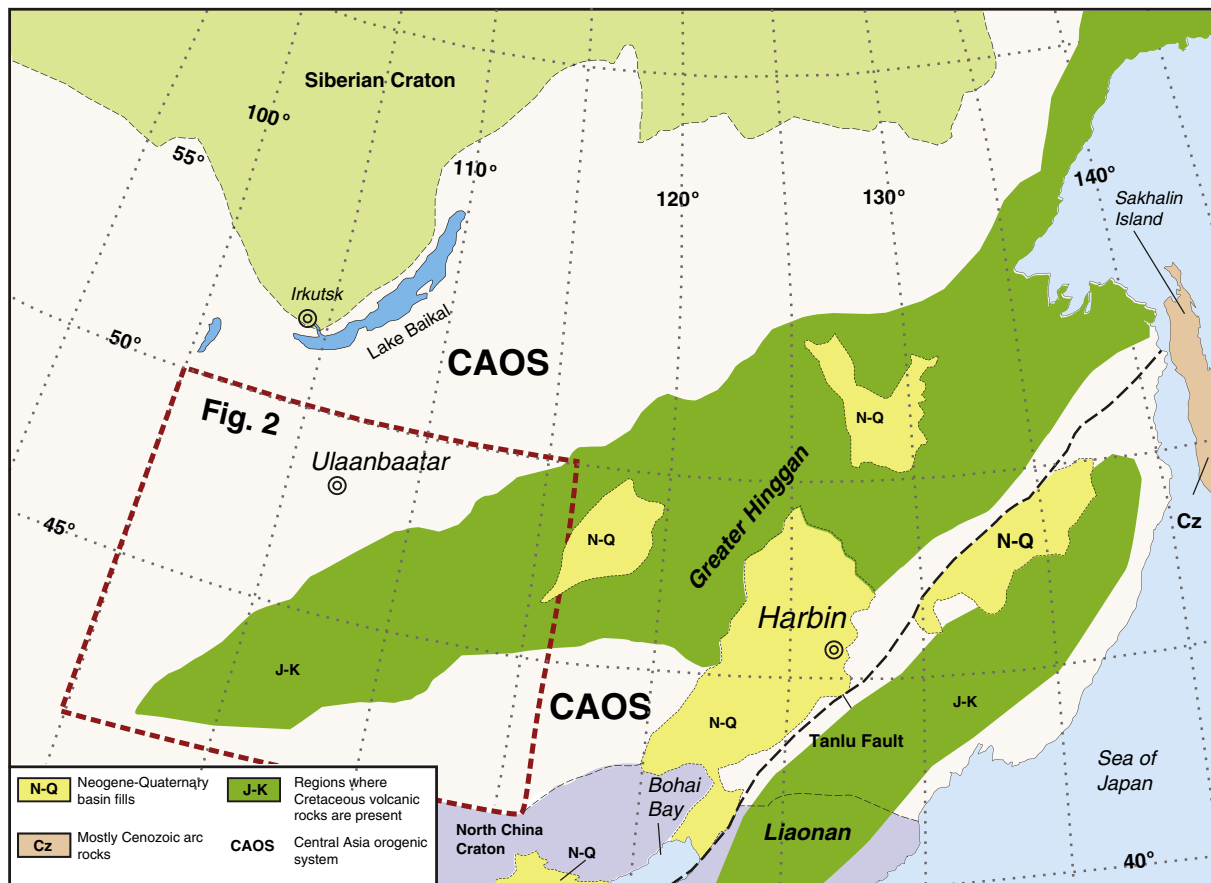


Fig. 1. Regions of Jurassic and Cretaceous volcanism superposed over the Central Asia Orogenic System (CAOS; also known as Central Asian Orogenic Belt or Central Asian accretionary orogen) in northeastern Asia. Geology is based on a compilation from Zonenshain et al. (1990), Li (2000), Badarch et al. (2002), and Wu et al. (2005a,b). Also shown is location of Fig. 2.

Despite being a prominent Mesozoic geologic feature, the origin of Cretaceous volcanism across a wide region of eastern Asia remains poorly understood. Existing hypotheses using geochemical and structural constraints were mostly constructed with the aim of explaining locally studied volcanic rocks. For example, models for the occurrence of Cretaceous volcanic rocks in eastern Mongolia and Siberia include (1) intra-continental rifting (Shatkov et al., 1980; Kovalenko and Yarmolyuk, 1990; Grahma et al., 2001), (2) formation of a continental arc resulting from westward subduction of the Pacific plate beneath Asia (Filippova et al., 1984; Zonenshain et al., 1990), and (3) mantle plume activities (Yarmolyuk et al., 1995). Similarly, models involving Cretaceous magmatism in the Greater Xing'an region of NE China (Fig. 1) emphasize the role of delamination (Wang et al., 2006), recycling of continental crust (Zhang et al., 2012), and regional extension (Wu et al., 2005b).

The southern segment of the Cretaceous volcanic zone in eastern Asia was well developed in SE China where four major episodes of igneous activities were documented during 136–146 Ma, 122–129 Ma, 101–109 Ma and 87–97 Ma (T.-D. Li, 2000; X.H. Li, 2000). T.-D. Li (2000), X.H. Li (2000) also noted that the coeval high-K calc-alkaline rocks have geochemical signatures similar to those formed in continental back-arc and post-collision extensional settings and that the eruption centers are spatially associated with extensional basins and basin-bounding normal faults. These observations again support the causal linkage between lithospheric extension and resulting volcanism (T.-D. Li, 2000; X.H. Li, 2000). Zhou et al. (2006) noted that Cretaceous tholeiitic basalts occurred in the interior of the South China Craton in a back-arc setting. They are interlayered with red beds in extensional basins and were interpreted by Zhou et al. (2006) as resulting from interaction of back-arc extension and upper-mantle melting.

In contrast to the well-studied Mesozoic volcanic rocks in eastern China, there have been no systematic investigations of Cretaceous volcanic rocks in eastern Mongolia and far-east Siberia. The lack of modern geologic research in this region has hindered testing of the aforementioned competing models for the origin of Cretaceous volcanism in eastern Asia. For example, the progressive delamination model of Wang et al. (2006) predicts that the initiation of Mesozoic volcanism occurred at the final closure site of the Mongol-Okhotsk Ocean and the volcanic front had migrated from west to east between 160 Ma and 110 Ma across NE China. In order to test the various competing models, we conducted a reconnaissance investigation of volcanic rocks in the far-eastern region of Mongolia directly west of the Mesozoic Greater Xing'an volcanic field of Wang et al. (2006) and J.H. Zhang et al. (2008), Zhang et al., 2010). Our work involves $^{40}\text{Ar}/^{39}\text{Ar}$ dating and geochemical analysis of Cretaceous volcanic rocks from this region (Fig. 2). Our new age result, together with the existing K–Ar ages, suggests that volcanism in eastern Mongolia occurred at 120–104 Ma. Our geochemical analysis indicates that the volcanic rocks were derived from a highly heterogeneous mantle source that is characterized by a mixture of depleted, enriched and metasomatized mantle. This geochemical characteristic can be explained by site-specific processes such as partial delamination of a previously thickened mantle lithosphere or mantle avalanche across the 670 phase boundary. It may also be explained by a regional tectonic process such as back-arc extension induced by westward subduction of the Pacific plate below Asia.

2. Geological setting

We identified three Cretaceous volcanic associations in eastern Mongolia: (1) a bimodal series, (2) a shoshonite series, and (3) a basanite Series. Our field work focuses mainly on collecting volcanic samples at

eight sites (Fig. 2). Below we describe the field occurrence, petrology, and relationships of our sample sites to local structures.

2.1. Bimodal series

We observed rock series consisting mostly of alkali basalt (i.e., trachybasalt of Le Maitre et al., 1989) at field sites (1) and (2) in Fig. 2. We also examined minor tholeiitic basalts and felsic lavas within the studied volcanic sequences (Nagibna, 1975; Frikh-Har and Luchitskaya, 1978). The volcanic rocks are spatially associated with northeast-trending extensional grabens that are 25–75 km wide and 75–200 km long (Dobrolubov and Flippova, 1990). The basalt sequences were deposited on top of fossil-bearing Cretaceous shale, sandstone, mudstones. The fossil ages place the earliest Cretaceous as the lower age bound for the eruption of the basaltic volcanic sequences (Dobrolubov and Flippova, 1990). The upper part of the volcanic sequences in the studied areas is composed of rhyolitic flows and tuff; in contrast, the lower part of the volcanic sections is composed dominantly of basaltic flows (Dobrolubov and Flippova, 1990). The basalt in the bimodal series yields K–Ar and Rb/Sr ages of ~120 Ma based on the previous studies (Solovyev et al., 1977a,b; Frikh-Har and Luchitskaya, 1978; Shuvalov, 1988).

2.2. Shoshonite series

Violet-colored shoshonite series rocks with porphyritic textures form calderas (Fig. 3). Their distribution is controlled by northeast-trending rifts and younger northwest-trending faults (Tauson et al., 1984a,b). The calderas are 0.75–1.5 km in diameter. Latite flows are also present in the volcanic sequence and contain variable amounts of phenocrysts with colors ranging from dark to pale violet. In some calderas, porphyritic felsic rocks occur as scorous latite and trachydacite. Shoshonite consisting of felsic flows and volcanic glass is black, reddish and greenish in color. Felsic volcanic rocks are composed of quartz latite, trachyte, trachydacite, and rhyolite. Volcanoclastic and tuffaceous rocks are also present in volcanic sequences. Shoshonite is spatially associated with narrow fault zones, whereas rhyolitic dikes fill conic extensional faults around calderas.

In the Tsagandelger area at field site (3) in Fig. 2, the volcanic rocks occur as calderas located with graben structures. They are composed of absarocite and shoshonite flows. In some cases, rhyolites occur above the upper part of the shoshonite flow with a similar relationship as the bimodal series mentioned above.

In the Choir area at field site (4) in Fig. 2, calderas constructed by shoshonite occur along northeast-trending extensional fault zones. Latite, trachydacite, rhyolites, and felsic tuff are also present in the volcanic sequences. Syenite dikes and fluorine veins are also present in the caldera complexes.

A single caldera occurs in the Tsav area at field site (5) in Fig. 2. It is constructed by volcanic flows, volcano-clastic deposits, and hypabyssal intrusive monzodiorite, monzonite, syenite and granitic porphyry (Baljinnyam et al., 1989; Dash, 1996). Veins containing silver–lead–zinc ores are the youngest features in this caldera. Pb–Pb dating of galena from the ore deposits yields an ore formation age of 98–110 Ma (Gantumur, 2005). Uranium and molybdenum deposits also occur in the shoshonite series. In the Tsagannur area at field sites (6) and (7) in Fig. 2, volcanic flows in calderas consist of latite, dacite and quartz monzonite.

The age of the shoshonite is not well determined and has been assigned to be either the Cretaceous (Yanshin, 1989) or Triassic–Jurassic (Tomurtogoo, 1999) in the existing regional geologic maps. A few K–Ar ages obtained from the shoshonite series are Cretaceous (Frikh-Har and Luchitskaya, 1978; Yanshin, 1978). Jakes and White (1972) and Morrison (1980) showed that shoshonite series emplaced after eruption of basaltic rocks in the bimodal series. Similarly, Kovalenko and Yarmolyuk (1990) proposed that the shoshonite is the youngest unit in the eastern Mongolia volcanic zone based on contact relationships they observed in the field.

2.3. Basanite series

Basanite occurs at field site (8) in Fig. 2 as small cinder cones composed of volcanic bombs, basaltic breccias, massive basaltic flows, and pumice. It is interbedded with sedimentary rocks and locally contains mantle xenoliths in volcanic flows. Makhbadar and Delgertsogt (1990) obtained Cretaceous ages from basalt using the K–Ar dating method.

3. Petrography

Shoshonite series rocks display porphyritic textures. Their phenocrysts include hypersthene, augite, amphibole, mica, and feldspar. The groundmass is black glass. Felsic volcanic rocks occur as quartz latite, trachyte, trachydacite, and rhyolite. Examples of mineral compositions under microscope are shown in Fig. 4. Olivine in a thin section from a trachybasalt sample shows that its grains are replaced by serpentine along their rims (Fig. 4A). Phenocrysts in the sample include magnetite,



Fig. 3. A field picture of a cinder cones in the Tsagandelger area. The volcanic flows defining the flanks of the cinder cones are shoshonite-series rocks.

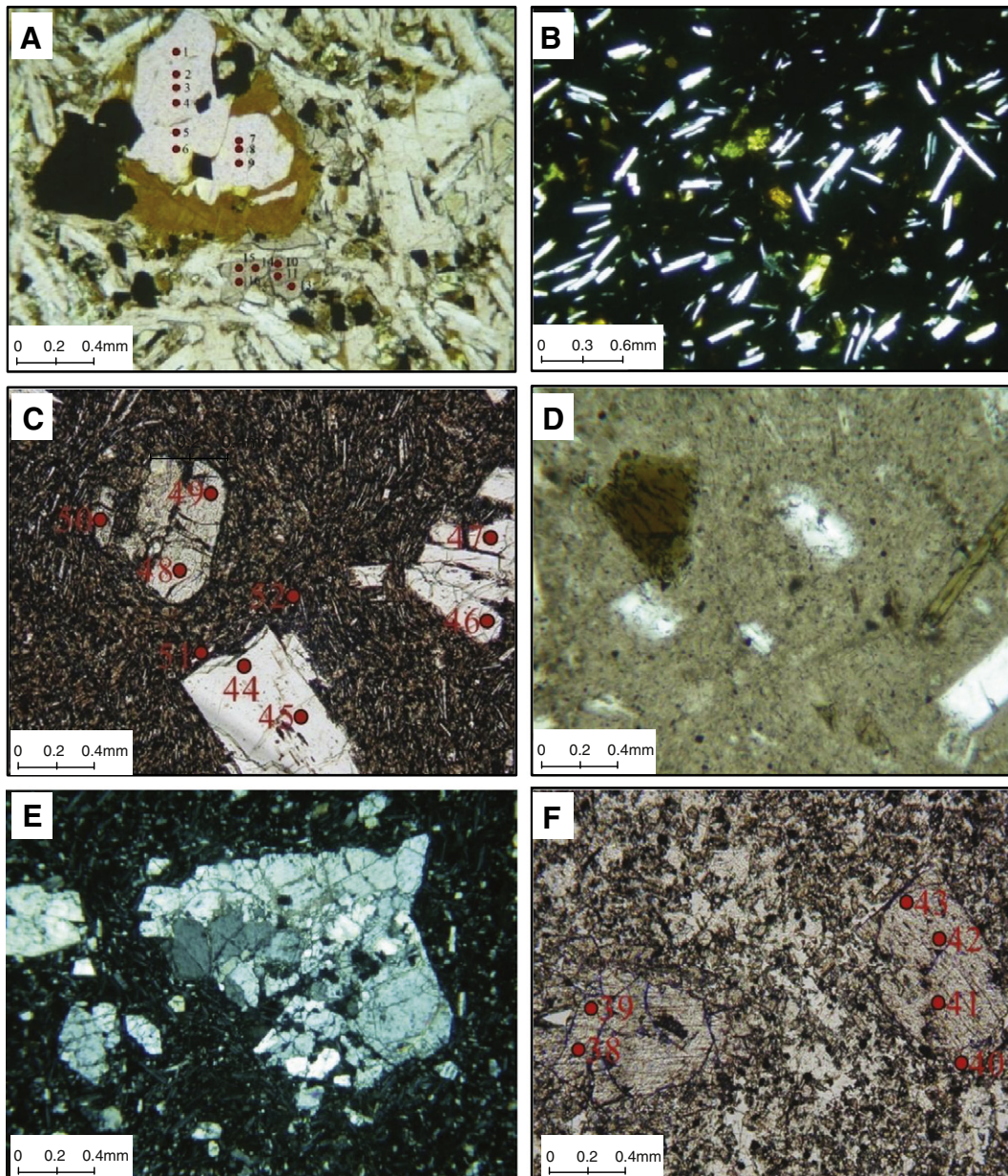


Fig. 4. (A) Olivine phenocrysts in a trachybasalt sample are replaced by serpentine along their rims. Major mineral phases in the sample include magnetite, subhedral augite (labeled at locations 10–15), poikilitic plagioclase, and pigeonite. (B) A thin section of a vitric basalt sample displays plagioclase, microlite, and small crystals of pigeonites embedded in the glassy ground mass. (C) A thin section of a shoshonite sample displays hypersthene (locations 46, 47, 48, 49, and 50) and plagioclase in the ground mass and plagioclase, microlites, augite, and magnetite as phenocrysts. (D) Mineral composition of a quartz latite sample includes hornblende, biotite, and plagioclase as phenocrysts and its ground mass consists of plagioclase, K-feldspar microlites, quartz, and magnetite. (E) Olivine in a basanite sample broke down into smaller fragments and its ground mass consists of plagioclase microlites, small crystals of olivine, and volcanic glass with normative nepheline. (F) A thin section of a basalt sample displays pigeonite (locations in 38 and 39) and diopsidic augite (locations 40, 41, 42, and 43) as phenocrysts. Its ground mass consists of plagioclase microlite, small crystals of augite, magnetite and volcanic glass with normative nepheline.

subhedral augite (labeled at locations 10–15 in Fig. 4A), poikilitic plagioclase, and pigeonite. A thin section of a vitric basalt sample displays plagioclase, microlites, and small crystals of pigeonites embedded in the blackish glass under microscope (Fig. 4B). Shoshonite samples are typically composed of hypersthene (locations 46, 47, 48, 49, and 50 in Fig. 4C) and plagioclase phenocrysts in the ground mass and plagioclase, microlite, augite, and magnetite as phenocrysts. The mineral composition of quartz latite is shown in a thin section in Fig. 4D, which includes hornblende, biotite, and plagioclase as phenocrysts; its ground mass consists of plagioclase, K-feldspar microlite, quartz, and magnetite. A thin section from a basanite sample shows that olivine broke down into smaller fragments and the ground mass of the sample consists of plagioclase microlite, small crystals of olivine, and volcanic glass with

normative nepheline (Fig. 4E). Finally, a thin section of a basalt sample displays pigeonite (locations in 38 and 39 in Fig. 4F) and diopsidic augite (locations 40, 41, 42, and 43 in Fig. 4F) as phenocrysts; its ground mass consists of plagioclase microlite, small crystals of augite, magnetite, and volcanic glass with normative nepheline.

4. Analytical techniques

4.1. Element and Sr–Nd isotope analyses

Whole-rock samples were ground in an agate mill, after careful washing in distilled water. Major elements were measured by XRF spectrometer on glass disks made by fusion of whole rock with lithium

metaborate. The FeO and Fe₂O₃ contents were analyzed by wet chemical analyses at the Central Geology Laboratory of Mongolia at Ulaanbaatar. Trace elements were analyzed by inductively coupled plasma-mass spectrometry (ICP-MS) at Key Laboratory for Mineral Resources Research, Institute of Geology and Geophysics, Chinese Academy of Sciences.

Whole-rock samples were analyzed for Sr and Nd isotopic compositions also at Key Laboratory for Mineral Resources Research, Institute of Geology and Geophysics, Chinese Academy of Sciences. Sr and Nd were extracted by conventional ion exchange chromatographic techniques, after dissolution with a HF–HNO₃–HCl mixture in closed Teflon bottle at 120 °C for 72 h. Sr and Nd isotopic ratios were measured using a Finnigan MAT-262 multiple-collector mass spectrometer, thermal ionization mass spectrometer running in dynamic mode. Blanks were on the order of <0.3 ng for Sr and 0.05 ng for Nd. Replicate analyses of the Sr NBS-987 and Nd La Jolla reference standards gave average values of ⁸⁷Sr/⁸⁶Sr = 0.7100287 ± 0.000010 (n = 14) and ¹⁴³Nd/¹⁴⁴Nd = 0.511942 ± 0.000012 (n = 12), respectively. The ⁸⁷Sr/⁸⁶Sr ratios were normalized within run to ⁸⁶Sr/⁸⁸Sr = 0.1194, and the ¹⁴³Nd/¹⁴⁴Nd ratios were normalized within run to ¹⁴⁶Nd/¹⁴⁴Nd = 0.7219. All errors and standard deviations are given at the 2 – σ level.

4.2. ⁴⁰Ar/³⁹Ar dating

⁴⁰Ar/³⁹Ar dating was conducted at the Noble Gas Laboratory of Arizona State University in 2009. Mineral separates and whole rock chips for ⁴⁰Ar/³⁹Ar analysis were first individually weighed and wrapped in aluminum foil. They were then stacked inside evacuated quartz glass tubes between GA1550 biotite (98.79 ± 0.54 Ma, [Renne et al., 1998](#)) and PP-20 hornblende (a re-preparation of standard Hb3g with an apparent age of 1072 Ma; [Roddick, 1983](#)) that served as flux monitors to calculate J-factors. K₂SO₄ and CaF₂ salts were used to calculate correction factors for interfering neutron reactions. The samples were irradiated for 30 h at the USGS TRIGA Reactor, Denver, Colorado. Resulting neutron flux was calculated ranging from 6.65E–3 to 6.68E–3 over the length of the stack. Following a 2 to 3 week cooling period to allow for the decay of short-lived isotopes, samples were loaded into the arms of a glass storage tree above a double-vacuum, resistance-heated furnace and heated to 120° at the same time that the entire extraction line was baked for 48 h at 220 °C. Getters and furnace were independently degassed near the end of the bake-out. Samples were then dropped into the furnace and argon was extracted from each sample using a computer controlled step-heating routine. The temperature of the furnace is estimated to be accurate to ± 20 °C. Each heating step had duration of 12 min followed by a cool down to 500 °C prior to advancing the gas into two successive gettering stages for argon purification. The argon was then admitted into a VG 5400 mass spectrometer, where it was ionized and detected by a VG electron multiplier and digitized with a Keithley 617 Electrometer. Data collection and processing were accomplished using the computer program Mass Spec ([Deino, 2001](#)). The decay constants used were those recommended by [Steiger and Jäger \(1977\)](#). Baseline values were subtracted and the isotopic measurements then were regressed to time zero using standard regression techniques. Additional corrections and associated uncertainties were applied to account for blanks, machine discrimination, atmospheric contribution, and interfering isotopes produced in the reactor from Ca, K and Cl present in the samples. Ages cited are at the 1 sigma level and do not include uncertainties in J factors or decay constants which generally range from 0.5 to 0.8%.

5. Results

5.1. Major elements

We analyzed 19 samples from the bimodal series that include basalt, trachybasalt, basaltic andesite, and basaltic trachyandesite ([Table 1](#)). Their SiO₂ contents range from 47.50 to 54.10 wt.%, with high contents

of TiO₂ (1.48–2.46 wt.%), Al₂O₃ (15.17–18.53), FeO_{total} (8.30–12.83 wt.%) and Na₂O + K₂O (3.52–6.35 wt.%) and low contents of MgO (2.78–4.44 wt.%). Their Mg# [= MgO/(MgO + FeO_{total}), molar ratio] and K₂O/Na₂O ratios vary in the ranges of 0.32–0.44 and 0.27–0.75, respectively.

We also analyzed 27 samples from the shoshonite series that include absarokite, shoshonite, latite, trachydacite, and trachyrhyolite. The results show a large variation in the SiO₂ contents (49.67 to 77.01 wt.%). The shoshonite series are characterized generally by very high Na₂O + K₂O (6.38–11.98 wt.%) contents and show varying K₂O/Na₂O ratios (0.88–3.44). One sample, however, yields an extremely high K₂O/Na₂O ratio of 33.23 ([Table 2](#)). Samples from absarokite, shoshonite, most latite, and some trachyrhyolite have high Mg# (0.32–0.52).

Fe₂O₃/FeO ratios of three rock series differ significantly ([Fig. 5](#)). Basanite and tephrite samples display low (<1.0) Fe₂O₃/FeO ratios varying little with SiO₂. In contrast, shoshonite samples display a high Fe₂O₃/FeO ratio (>1), indicating their occurrence in a reducing environment or during dehydration of subducted materials in a mantle wedge.

The 9 samples from the basanite series have very low contents of SiO₂ (40.72–44.06 wt.%) but high contents of TiO₂ (2.10–3.52 wt.%), FeO_{total} (9.32–12.37 wt.%), MgO (5.27–10.78 wt.%), CaO (7.92–11.02 wt.%). The samples also show very high contents of Na₂O + K₂O (5.36–7.51 wt.%) that are associated with high Mg# (0.48–0.67) and low K₂O/Na₂O ratios (0.18–0.33).

In addition to the basanite and tephrite from the basanite series, which have low SiO₂ (40.72–44.06 wt.%) and K₂O (1.22–1.96 wt.%) contents, the samples from the bimodal series have K₂O contents of 0.98–2.69 wt.% and thus they are mostly plotted in the field of high-K calc-alkaline series, with five in the field of shoshonite series and two in the field of medium-K calc-alkaline series, whereas most samples from the shoshonite series are plotted in the field of shoshonite series, with three in the field of high-K calc-alkaline series ([Fig. 6; Table 3](#)).

5.2. Trace elements

In general, the chondrite-normalized REE (rare earth elements) patterns of the samples from the bimodal series show higher U contents than Th contents. Elements Cs, Ba, and U display positive anomalies whereas elements Nb and Ta show negative anomalies ([Fig. 7](#)). The REE patterns also show LREE (light REE) enrichment, with slightly negative Eu anomalies ([Fig. 8](#)).

The absarokite and shoshonite samples from the shoshonite series show similar REE patterns to the basalt samples from the bimodal series ([Fig. 9](#)), generally with LREE enrichment and slightly negative Eu anomalies. These samples generally have higher REE contents than the latite, trachydacite, and rhyolite samples in the same series ([Table 2](#)). Although all of the samples from the shoshonite series have wide ranging U and Th contents and show Nb and Ta negative anomalies ([Fig. 10](#)), the rhyolite samples have more significantly negative Sr and Eu anomalies than the other samples.

The basanite and tephrite samples from the basanite series show parallel REE patterns, with LREE enrichment and insignificant Eu anomalies ([Fig. 11](#)), and they also have parallel trace element patterns normalized to the primitive mantle ([Fig. 12](#)). Both types of rocks show positive Nb, Ta, and Sr anomalies and negative Cs, Rb, and Pb anomalies, in contrast to those from the bimodal and shoshonite series ([Fig. 12](#)).

When the basaltic samples are averaged and plotted together, the basanite series have the REE patterns resembling those for absarokite and shoshonite from the shoshonite series, characterized by lower LREE and higher HREE (high REE) contents than those from the bimodal series, whereas latite has the lowest HREE contents ([Fig. 13](#)). In addition, the three series can be distinguished from each other by their Ta and Nb anomalies. Specifically, absarokite and shoshonite from the shoshonite series have most depleted contents of Ta and Nb, whereas the basanite series are characterized enrichment in the contents of Ta and Nb; the contents of Ta and Nb for basaltic samples from the bimodal series lie in between ([Fig. 14](#)).

Table 1
Chemistry of the bimodal series alkali basalt.

Rock name	Basalt		Trachybasalt						Basaltic-andesite		Basaltic-trachyandesite								
	2/5	1/1	1/2	6/8	1/15	6/6	1/8	6/1	2/4	6/7	6/3	1/7	2/6	2/1	2/11	1/15-1	6/4	6/2	6/5
Sample N	112.20.54	107.13.52	107.11.57	115.23.13	107.31.49	115.19.9	107.25.56	115.17.46	112.15.01	115.22.14	115.17.35	107.32.35	110.16.43	112.13.38	108.59.53	107.36.8	115.15.56	115.15.18	115.15.18
Longitude	112.20.54	107.13.52	107.11.57	115.23.13	107.31.49	115.19.9	107.25.56	115.17.46	112.15.01	115.22.14	115.17.35	107.32.35	110.16.43	112.13.38	108.59.53	107.36.8	115.15.56	115.15.18	115.15.18
Latitude	46.59.05	47.7.12	47.9.12	48.50.15	46.21.20	48.52.14	46.51.52	48.59.39	46.25.58	48.52.34	48.57.11	46.43.58	46.54.25	47.00.38	47.11.37	46.19.29	48.54.55	48.58.44	48.53.40
SiO ₂	49.34	47.85	47.50	50.83	50.96	51.59	51.74	51.83	52.14	52.38	52.17	52.48	52.66	52.71	52.73	53.15	53.18	53.74	54.1
TiO ₂	2.11	2.43	2.31	2.16	2.46	2.19	2.07	2.07	2.15	2.32	2.25	2.41	1.95	2.12	1.48	2.43	2.1	2.02	2.18
Al ₂ O ₃	18.53	15.24	15.17	16.13	15.33	16.16	16.02	16.32	16.14	16.37	16.21	16.09	16.14	15.42	15.99	15.5	16.25	15.34	15.21
Fe ₂ O ₃	2.63	4.00	3.83	5.46	4.00	4.68	2.45	2.54	4.97	2.69	3.56	2.81	3.4	2.85	1.27	4.25	2.51	2.66	4.27
FeO	8.24	8.85	9.38	6.08	6.69	6.10	6.09	7.57	6.40	8.38	5.98	5.86	6.57	6	7.27	7.00	8.95	8.1	5.48
MnO	0.17	0.15	0.15	0.12	0.06	0.18	0.14	0.16	0.14	0.17	0.21	0.14	0.13	0.15	0.15	0.07	0.07	0.38	0.23
MgO	4.44	4.33	4.25	3.94	3.66	3.48	3.65	3.40	3.58	3.50	3.38	3.58	3.88	3.61	3.37	3.87	2.93	2.78	2.86
CaO	7.72	7.05	7.21	6.66	6.20	6.17	6.71	6.11	6.33	6.17	6.24	6.73	6.37	6.46	6.95	6.51	5.61	5.76	4.95
Na ₂ O	2.40	2.83	3.61	3.90	3.48	3.61	4.40	3.54	3.09	3.62	3.65	4.4	4.6	3.24	3.95	3.55	3.32	3.28	3.38
K ₂ O	1.12	1.94	1.95	1.65	2.47	2.69	1.95	2.65	1.16	0.98	2.42	1.75	1.72	2.1	1.52	2.08	2.24	2.42	2.4
P ₂ O ₅	0.34	1.52	1.49	0.53	0.69	1.01	0.67	0.89	1.79	0.98	1.35	0.66	0.55	0.96	0.62	0.54	1.21	0.84	1.39
LOI	2.73	3.56	1.73	2.45	2.57	2.19	3.56	2.92	1.26	2.52	2.47	3.07	2.16	4.15	3.93	1.03	1.65	2.68	3.52
Σ	99.77	99.75	98.58	99.91	98.57	100.05	99.45	100.00	99.59	100.08	99.89	99.98	100.13	99.77	99.23	99.98	100.02	100	99.97
Fet	10.87	12.85	13.21	11.54	10.69	10.78	8.54	10.11	11.37	11.07	9.54	8.67	9.97	8.85	8.54	11.25	11.46	10.76	9.75
Fet/Mg	2.45	2.97	3.11	2.93	2.92	3.10	2.34	2.97	3.18	3.16	2.82	2.42	2.57	2.45	2.53	2.91	3.91	3.87	3.41
Fe ₂ O ₃ /FeO	0.32	0.45	0.41	0.90	0.60	0.77	0.40	0.34	0.78	0.32	0.60	0.48	0.52	0.48	0.17	0.61	0.28	0.33	0.78
Na + K	3.52	4.77	5.56	5.55	5.95	6.30	6.35	6.19	4.69	4.60	6.07	6.15	6.32	5.34	5.47	5.63	5.56	5.70	5.78
K/Na	0.47	0.69	0.54	0.42	0.71	0.75	0.44	0.75	0.52	0.27	0.66	0.40	0.37	0.65	0.38	0.59	0.67	0.74	0.71
<i>ppm</i>																			
Co	23.5	28.4	20.6	22.5	25.0	44.2	23.8	20.2	18.4	28.8	47.9	25.1	40.1	22.8	27.3	24.4	43.2	17.6	43.8
Ni	48.2	50.7	37.6	42.2	64.5	37.6	41.7	45.5	54.8	47.6	28.6	36.8	25.2	24.8	28.6	30.1	23.2	32.6	21.2
Ga	23.4	23.2	22.1	24.6	24.2	20.9	24.7	21.3	22.3	22.7	19.8	23.4	20.55	21.7	23.4	21.5	24.1	21.9	19.7
Rb	146.5	54.7	92.9	90.7	63.5	59.3	142.7	70.1	91.2	90.7	65.6	117.7	85.9	83.8	41.8	49.2	95.8	65.5	21.5
Sr	850.7	841.4	570.1	858.0	1140	810	855.5	539.5	886.3	880	710	746.8	828	819.7	763.8	727.2	880	734.3	802.3
Y	43.2	32.6	29.4	41.8	33.1	41.7	42.3	43.9	44.3	42.6	42.6	49.6	47.1	21.2	26.5	32.8	47.5	43.2	29.5
Zr	442.8	366.3	365.3	401.5	482.8	360.8	443	384.3	355.4	380.1	320.6	409.2	365.2	303.9	422.7	386.1	314.7	321.4	341.2
Nb	34.5	31.7	24.1	38.8	29.0	41.2	32.9	33.3	40.1	41.2	40.6	39.4	36.6	23.4	21.8	30.64	38.56	34.40	27.4
Cs	1.27	1.06	3.51	1.26	1.77	1.25	2.39	1.77	1.25	1.68	1.34	3.27	1.56	2.22	1.14	1.21	2.70	1.36	2.91
Ba	1023.5	1040	817.2	857.7	1462.1	1300	1196.8	1017.8	986.2	956.8	1500	1177.7	1008.5	879.3	1226.6	951	1300	1107.1	914
Hf	7.85	8.43	9.26	9.28	11.22	9.86	10.9	9.75	8.45	8.78	8.57	9.94	9.58	7.15	7.13	10.28	10.56	7.61	3.53
Ta	2.21	1.62	1.81	2.41	1.51	2.27	1.92	2.07	2.54	2.47	2.24	2.33	2.84	1.38	1.82	1.43	2.16	2.13	0.48
Pb	24.5	12.5	19.0	21.2	19.31	23.3	18.38	14.24	14.5	16.9	10.5	13.62	17.8	13.59	12.55	18.5	11.4	10.55	6.57
Th	4.38	2.88	8.26	4.28	4.31	4.12	4.07	4.35	4.34	4.31	4.66	4.21	4.18	4.04	6.36	4.14	4.08	4.59	4.21
U	1.83	1.24	3.09	2.20	1.16	2.5	1.08	1.11	5.45	2.18	1.63	1.09	2.65	1.07	1.14	2.26	2.55	1.58	1.67
La	53.42	63.81	65.64	58.27	76.04	54.1	63.21	50.71	55.48	52.9	64.7	52.96	54.72	47.87	58.54	74.41	64.7	50.42	38.2
Ce	113.8	134.4	139.33	124.8	161.02	114.3	134.66	106.99	117.4	112.3	137.3	110.15	115.5	99.26	120.12	155.6	135.6	105.96	80.9
Pr	18.54	18.50	16.84	21.5	22.18	14.4	19.51	14.33	18.44	20.7	20.2	14.59	14.83	12.67	15.85	16.2	15.8	13.63	10.34
Nd	56.22	74.17	61.76	58.6	86.9	52.6	74.11	56.26	64.8	60.5	74.80	56.63	71.45	46.32	58.96	82.70	68.76	53.28	44.71
Sm	10.41	14.96	11.29	11.56	18.07	9.90	14.99	12.61	11.2	12.35	12.6	12.45	10.9	8.83	9.71	16.26	11.73	11.52	8.30
Eu	2.72	2.88	1.97	2.75	3.95	2.84	3.19	2.66	3.28	2.74	3.34	2.87	3.19	2.19	2.70	3.23	2.65	2.75	2.34
Gd	10.15	10.53	9.02	11.40	13.31	10.3	11.91	10.16	12.12	10.34	12.1	11.25	11.45	8.95	8.45	11.48	10.54	9.64	7.51
Tb	1.52	1.46	1.28	1.63	1.69	1.51	1.67	1.58	1.60	1.62	1.64	1.72	1.55	0.95	1.23	1.55	1.57	1.53	1.06
Dy	9.05	7.22	6.63	8.85	7.93	8.3	9.02	9.33	8.54	9.12	8.21	9.42	8.41	4.87	5.88	7.41	9.42	8.53	5.17
Ho	1.74	1.28	1.25	1.84	1.36	1.76	1.71	1.85	1.73	1.76	1.83	1.91	1.68	0.84	1.13	1.26	1.73	1.72	1.02
Er	4.23	3.18	3.18	4.47	3.37	3.91	4.4	4.81	4.28	4.1	4.14	5.01	3.86	2.18	2.39	3.12	4.50	4.45	2.81
Tm	0.62	0.42	0.45	0.65	0.44	0.63	0.60	0.67	0.65	0.72	0.62	0.71	0.65	0.31	0.35	0.41	0.68	0.64	0.42
Yb	3.58	2.58	2.76	4.05	2.69	4.22	3.77	4.29	4.26	4.37	3.90	4.39	3.63	1.93	1.97	2.64	4.28	3.94	2.62
Lu	0.56	0.37	0.42	0.62	0.38	0.64	0.57	0.65	0.58	0.63	0.55	0.68	0.61	0.28	0.33	0.38	0.63	0.61	0.36

Table 2
Chemistry of the shoshonite series rocks.

Rock name	Absarokite	Absarokite	Absarokite	Shoshonite	Shoshonite	Shoshonite	Shoshonite	Shoshonite	Shoshonite	Latite	Latite	Latite	Latite
Sample N	4/4	3/23	4/1	3/527	4/2	6/199	3/12	4/626	3/11	4/620	3/14	4/625	3/45
Longitude	109.1.41	107.52.16	109.47.25	107.47.53	109.22.34	115.19.38	107.45.26	109.13.52	107.44.39	109.52.16	107.46.53	109.48.19	107.53.17
Latitude	46.10.27	46.29.49	46.11.1	46.13.39	46.13.2	48.55.37	46.20.4	46.11.16	46.20.2	46.15.35	46.17.28	46.13.32	46.15.48
SiO ₂	49.67	50.4	51.51	52.24	53.71	54.58	55.18	55.35	55.41	56.13	56.68	57.85	58.3
TiO ₂	2.2	2.12	2.14	2.10	2.15	1.46	1.50	1.55	1.42	1.68	0.97	1	1.34
Al ₂ O ₃	17.09	17.52	16.92	18.05	15.81	15.51	17.59	16.22	17.92	16.92	16.24	16.63	17.78
Fe ₂ O ₃	7.72	5.38	5.0	7.56	5.2	5.7	4.73	4.45	4.19	4.3	3.37	4.1	3.28
FeO	2.43	4.25	4.29	2.31	3.40	2.6	3.34	4.2	2.85	3.21	2.95	2.2	2.96
MnO	0.15	0.13	0.14	0.08	0.12	0.11	0.06	0.35	0.09	0.66	0.1	0.1	0.06
MgO	4.18	3.86	3.75	3.84	3.08	3.45	3.65	2.23	2.28	3.08	3.41	3.11	1.8
CaO	6.26	5.71	6.72	5.21	5.67	4.02	6.27	6.09	5.76	5.24	5.69	5.44	5.79
Na ₂ O	3.69	3.24	3.42	3.81	3.41	3.43	3.44	2.93	3.46	3.23	3.64	3.67	3.54
K ₂ O	3.93	3.37	2.96	3.35	3.11	4.25	3.16	3.52	3.56	3.47	4.07	3.95	3.62
P ₂ O ₅	0.95	0.95	1.15	0.59	0.74	0.78	0.69	0.61	0.47	0.22	0.33	0.57	0.38
LOI	1.54	2.65	1.92	0.9	3.04	3.8	0.41	2.43	2.48	1.82	2.65	1.2	1.1
Σ	99.81	99.58	99.92	100.04	99.44	99.69	100.02	99.93	99.89	99.96	100.1	99.82	99.95
Fet	10.15	9.63	9.29	9.87	8.60	8.30	8.07	8.65	7.04	7.51	6.32	6.30	6.24
Fet/Mg	2.43	2.49	2.48	2.57	2.79	2.41	2.21	3.88	3.09	2.44	1.85	2.03	3.47
Fe ₂ O ₃ /FeO	3.18	1.27	1.17	3.27	1.53	2.19	1.42	1.06	1.47	1.34	1.14	1.86	1.11
Na + K	7.62	6.61	6.38	7.16	6.52	7.68	6.6	6.45	7.02	6.7	7.71	7.62	7.16
K/Na	1.07	1.04	0.87	0.88	0.91	1.24	0.92	1.20	1.03	1.07	1.12	1.08	1.02
ppm													
Co	28.5	24.1	22.2	26.3	18.4	38.4	18.4	24.0	13.6	16.1	17.4	16.8	7.91
Ni	56	120	79	122	76	110	75	43	65	47.6	33.8	41.2	15.5
Ga	24.9	23.3	22.7	24.1	22.3	23.2	23.4	21.8	21.5	22.2	22.1	24.3	21.8
Rb	116.1	117.5	120.5	116.8	97.4	96.1	54.3	78.0	71.3	73.3	61.1	68.4	71.8
Sr	820.3	877.6	936.9	848.95	725	959.2	1102.7	874	962.6	973.4	892.1	956.3	715.7
Y	30.90	31.8	30.5	31.35	28.3	33.09	17.73	19.22	17.54	18.1	17.5	16.0	29.8
Zr	495	437.3	427.5	466.15	415	458	340.2	286	227.5	240.1	247.2	314.0	213.2
Nb	28.9	23.1	20.8	25.95	18.2	22.3	15.3	16.4	8.7	6.70	9.33	12.12	14.70
Cs	2.05	2.77	4.94	2.41	1.32	1.12	1.15	1.19	1.96	1.21	1.26	1.57	3.84
Ba	1053.8	931.8	1096.7	992.8	974.1	1201	1011	1144	820.1	813.2	1221.9	1005	1096.4
Hf	11.84	10.37	9.84	11.11	9.47	11.60	7.93	11.35	5.77	6.64	6.26	8.31	6.82
Ta	1.61	1.27	1.14	1.44	0.99	1.62	0.74	0.45	0.49	0.38	0.51	0.55	0.97
Pb	17.61	16.68	16.75	17.52	18.18	15.66	17.42	24.12	14.35	24.40	16.28	18.37	22.42
Th	5.82	6.99	5.39	6.41	6.88	9.33	6.57	7.16	6.34	6.56	7.85	6.21	4.11
U	3.21	1.57	1.27	2.29	1.57	2.32	1.25	1.64	1.47	1.52	1.57	1.18	2.32
La	82.94	78.03	75.64	80.49	72.41	75.2	65.37	91.4	39.65	80.17	44.42	86.29	68.31
Ce	169.14	163.96	158.55	148.55	144.5	146.4	131.02	175.1	80.03	158.51	85.13	148.21	117.74
Pr	22.05	20.99	20.18	21.52	17.9	18.37	16.38	21.06	10.09	15.13	10.54	17.30	13.9
Nd	80.97	80.18	73.19	80.58	63.41	69.7	57.81	75.8	36.51	52.06	37.33	60.27	46.42
Sm	15.03	14.27	13.57	14.65	11.45	11.6	9.92	14.1	6.83	9.22	6.83	11.09	8.35
Eu	3.02	2.99	2.77	3.01	2.41	2.38	2.32	3.1	1.75	1.21	1.59	2.27	1.55
Gd	12.13	10.89	10.87	11.51	9.27	9.11	7.20	14.4	5.31	7.42	5.28	7.95	6.86
Tb	1.51	1.45	1.38	1.48	1.21	1.29	0.89	1.67	0.71	0.88	0.72	0.81	0.97
Dy	7.24	7.23	6.77	7.25	5.94	5.78	4.24	7.97	3.75	4.10	3.63	3.8	5.63
Ho	1.32	1.31	1.27	1.31	1.12	1.08	0.76	1.44	0.72	0.68	0.71	0.62	1.13
Er	3.33	3.33	3.25	3.32	2.89	2.94	1.82	3.40	1.86	1.60	1.81	1.30	3.15
Tm	0.43	0.47	0.43	0.45	0.39	0.43	0.24	0.41	0.27	0.25	0.27	0.17	0.48
Yb	2.56	2.86	2.62	2.71	2.44	2.65	1.46	2.56	1.69	1.52	1.67	1.12	2.86
Lu	0.38	0.43	0.39	0.39	0.36	0.40	0.21	0.41	0.26	0.22	0.24	0.17	0.46

5.3. Sr–Nd isotopes

The three series show different Sr–Nd isotopic features (Fig. 15). For the basaltic rocks from the bimodal series, their measured $^{87}\text{Sr}/^{86}\text{Sr}$ and $^{143}\text{Nd}/^{144}\text{Nd}$ ratios are in the ranges of 0.705210 to 0.706000 and 0.512400 to 0.512713, respectively. Their initial $^{87}\text{Sr}/^{86}\text{Sr}$ and $^{143}\text{Nd}/^{144}\text{Nd}$ ratios, when they are corrected to 116 Ma, range from 0.70474 to 0.70548 and 0.51240 to 0.51262, respectively. The shoshonite series show a very large variation in the measured $^{87}\text{Sr}/^{86}\text{Sr}$ ratios (0.705600–0.73290), in which two trachyrhyolite samples have the extremely high $^{87}\text{Sr}/^{86}\text{Sr}$ ratios of 0.767100 and 0.732900, respectively, and the remaining $^{87}\text{Sr}/^{86}\text{Sr}$ ratios vary in a relatively narrow range of 0.705600–0.708300, but all the samples show little variation in $^{143}\text{Nd}/^{144}\text{Nd}$ ratios (0.512500–0.512703). Generally, the absarokite and shoshonite are characterized by low initial ratios of $^{87}\text{Sr}/^{86}\text{Sr}$ (0.70529–0.70608), whereas the latite has higher initial ratios of $^{87}\text{Sr}/^{86}\text{Sr}$ (0.70549–0.70775), and the highest initial ratios of $^{87}\text{Sr}/^{86}\text{Sr}$ (0.70760–

0.73377) are produced by quartz latite, trachyte, and trachyrhyolite, showing an increase with increasing SiO₂ contents. The basanite series have low $^{87}\text{Sr}/^{86}\text{Sr}$ ratios (0.704152–0.704384) and high $^{143}\text{Nd}/^{144}\text{Nd}$ ratios (0.512709–0.512788). Correspondingly, their initial $^{87}\text{Sr}/^{86}\text{Sr}$ and $^{143}\text{Nd}/^{144}\text{Nd}$ ratios show little variations: ($^{87}\text{Sr}/^{86}\text{Sr}$)_i = 0.70404–0.70431 and ($^{143}\text{Nd}/^{144}\text{Nd}$)_i = 0.51264–0.51272, respectively.

5.4. Ages of volcanic rocks

Two samples were used to date the ages of volcanic rocks (see Supplemental materials for data tables): one is shoshonite collected from the Tsagandelger area and the other basanite collected from the Dych Gol area. Apparent ages of all the steps of the shoshonite show an incremental increase with increasing temperature. A plateau age of 114 ± 0.7 Ma was given from steps 8 to 20 (Fig. 16A), the proportional ^{39}Ar of which is about 40%. The corresponding anti-isochron age is 114 ± 0.7 Ma with a Nier value of 295, showing no excess ^{40}Ar .

Q-latite	Q-latite	Q-latite	Q-latite	Q-latite	Tr. Dacite	Tr. Rhyolite						
7/130-1	3/9	7/128	3/5	7/130	3/21	3/6262	4/613	4/145	6/22	6/351	4/1561	3/10
116.28.9	107.39.20	116.27.15	107.47.13	116.28.27	107.46.20	107.46.40	109.9.19	109.55.20	115.19.29	115.19.23	109.50.6	107.43.24
49.54.56	46.24.53	49.54.31	46.15.03	49.55.22	46.17.09	46.15.41	46.7.60	46.12.12	48.55.58	48.55.45	46.11.54	46.23.44
60.95	61.56	62.65	64.8	65.07	68.75	70.45	70.59	71.14	71.26	72.34	77.35	77.01
0.64	0.67	0.87	0.65	0.48	0.18	0.28	0.37	0.01	0.28	0.39	0.01	0.13
16.59	17.11	16.11	16.04	15.32	12.86	13.91	14.28	12.53	14.05	13.58	12.17	11.38
4.02	3.53	3.5	4.4	2.58	0.98	1.00	0.87	1.40	1.22	1.52	0.35	1.36
0.81	1.2	1.07	2	1.03	0.56	0.79	0.40	0.43	0.52	0.48	0.22	0.10
0.14	0.06	0.1	0.07	0.03	0.05	0.01	1.24	0.3	0.01	0.04	0.01	0.01
1.64	0.41	2.09	0.55	1.02	0.18	0.51	0.41	0.46	0.21	0.48	0.33	0.02
3.81	2.56	3.26	1.43	2.6	0.93	1.58	1.43	1.67	0.25	0.81	0.30	0.09
3.81	3.71	3.55	3.86	3.84	4.10	3.70	3.99	3.78	0.35	3.6	2.76	2.02
4.35	4.47	4.49	4.78	4.26	5.24	4.55	4.05	4.22	11.63	5.64	4.97	6.95
0.31	0.33	0.3	0.2	0.11	0.03	0.10	0.55	0.81	0.01	0.07	0.67	0.02
2.88	2.3	1.80	1.17	3.65	4.91	1.71	1.83	2.62	0.2	1.0	0.04	0.75
99.95	97.91	99.79	99.95	99.99	98.77	98.59	99.98	99.37	99.99	99.95	99.18	99.84
4.83	4.73	4.57	6.40	3.61	1.54	1.79	1.27	1.83	1.74	2.00	0.57	1.46
2.95	11.54	2.19	11.64	3.54	8.56	3.51	3.10	3.98	8.29	4.17	1.73	73.00
4.96	2.94	3.27	2.20	2.50	1.75	1.27	2.18	3.26	2.35	3.17	1.59	13.60
8.16	8.18	8.04	8.64	8.1	9.34	8.25	8.04	8	11.98	9.24	7.73	8.97
1.14	1.20	1.26	1.24	1.11	1.28	1.23	1.02	1.12	33.23	1.57	1.80	3.44
ppm												
5.90	3.44	5.42	1.57	13.9	1.6	3.5	3.1	1.2	1.4	8.3	2.2	4.4
45.3	25.0	63.9	68.6	43.1	4.2	7.4	5.2	6.1	4.3	3.9	1.2	2.1
20.4	19	20.7	17.2	18.1	17.3	19.8	18.9	12.3	18.3	19.1	14.7	15.4
101.4	75.8	136.3	220.5	118.0	154.3	116.8	114.0	128.5	807.4	211.2	170.2	99.3
569.4	401.2	563	51.7	853.6	210.5	406.4	388.6	70.3	61.2	215.7	40.1	494.9
22.1	17.8	21.8	26.3	16.4	13.5	8.8	13.1	10.4	31.8	22.6	11.3	27.7
232.3	262.4	239.5	176.8	187.3	171.9	176.2	178.0	110.4	275.5	251.5	120.5	149.9
11.35	9.31	11.60	24.22	8.74	12.6	5.8	5.6	4.1	18.7	21.3	8.3	10.8
7.21	1.36	10.34	7.27	11.25	3.57	2.68	2.68	11.13	31.74	8.60	2.23	3.16
1031.1	1688.2	1142.7	221.8	1332.4	1080.0	1223.6	813.0	590.5	1022.0	605.3	409.7	482.1
6.33	6.78	6.48	6.76	5.45	5.47	4.92	4.54	4.27	7.81	7.83	3.80	4.43
0.87	0.61	0.9	2.47	0.84	1.03	0.46	0.38	0.21	1.36	3.42	2.80	0.84
29.45	19.55	30.11	43.54	33.72	33.17	28.4	25.7	26.5	49.3	21.70	24.12	282.1
11.55	7.88	11.88	23.26	17.29	19.8	14.37	13.2	9.6	20.8	40.73	23.85	10.8
2.89	1.77	2.46	5.98	3.99	4.69	1.99	2.96	4.09	4.60	5.14	4.27	2.86
41.23	37.94	42.06	37.87	37.69	59.8	40.21	48.04	37.0	50.7	64.2	68.5	28.9
83.77	73.99	83.64	74.84	70.65	105.13	68.18	78.1	60.5	104.6	116.8	132.8	61.3
10.33	9.37	10.56	9.18	8.21	11.12	7.33	9.30	5.64	12.44	13.59	16.12	7.10
36.71	33.53	38.31	32.08	28.12	34.74	22.21	37.37	18.18	46.30	46.61	57.12	27.16
7.02	6.23	7.42	6.71	5.11	5.06	3.29	6.60	2.84	8.17	7.25	10.0	4.91
1.51	1.46	1.56	0.33	1.17	0.90	0.63	1.31	0.51	1.39	1.04	1.05	0.80
5.54	4.75	5.88	5.55	4.04	3.82	3.24	5.87	2.52	6.15	4.94	10.09	4.71
0.79	0.69	0.83	0.93	0.53	0.51	0.43	0.72	0.31	1.05	0.83	1.44	0.78
4.22	3.65	4.24	5.64	2.81	2.32	1.88	3.73	1.42	5.12	3.79	7.60	4.34
0.85	0.45	0.86	1.17	0.55	0.46	0.34	0.67	0.28	1.07	0.73	1.33	0.95
2.32	2.11	2.19	3.38	1.55	1.34	0.88	1.63	0.74	3.08	2.03	2.9	2.72
0.36	0.34	0.33	0.52	0.25	0.22	0.15	0.18	0.11	0.48	0.32	0.38	0.42
2.38	2.08	2.14	3.37	1.66	1.48	1.12	0.91	0.74	3.11	2.16	2.12	2.66
0.37	0.32	0.31	0.5	0.25	0.22	0.18	0.13	0.11	0.48	0.32	0.33	0.42

Apparent ages for the basanite show a broad 'n' shape distribution, which means that the core of the mineral might be subjected to ^{40}Ar loss. A plateau age of 104 ± 0.3 Ma as yielded from the steps 5 to 10 (Fig. 16B), the proportional ^{39}Ar of which is about 50%. The corresponding anti-isochron age is 104 ± 0.7 Ma with a Nier value of 280, showing slight loss of ^{40}Ar .

6. Discussion

It is well known that Cretaceous volcanism had occurred over a wide region of eastern Asia (Shatkov et al., 1980; Filippova et al., 1984; Kovalenko and Yarmolyuk, 1990; Yarmolyuk et al., 1995; T.-D. Li, 2000; X.H. Li, 2000; Wu et al., 2005b). However, the origin of this volcanic belt remains intensely debated and has been attributed to a large

variety of models that include (1) intra-continental rifting, (2) deamination of a thickened mantle lithosphere generated by early orogenic processes, (3) back-arc extension, (4) recycling of continental crust, and (5) plume activities (e.g., Shatkov et al., 1980; Filippova et al., 1984; Kovalenko and Yarmolyuk, 1990; Yarmolyuk et al., 1995; T.-D. Li, 2000; X.H. Li, 2000; Wu et al., 2005b; Wang et al., 2006; Zhou et al., 2006; Zhang et al., 2012). One of the major obstacles to testing the above models is the lack of geochronological and geochemistry data from the remote and little studied eastern Mongolia and Siberia in northeastern Asia. Our work represents one of the first efforts in this regard by providing new age and geochemical data of Cretaceous volcanic rocks in this remote region. Specifically, our new $^{40}\text{Ar}/^{39}\text{Ar}$ ages and published K–Ar ages (Solovyev et al., 1977a,b; Frikh-Khar and Luchitskaya, 1978; Yanshin, 1978; Shuvalov, 1988; Dobrolubov and

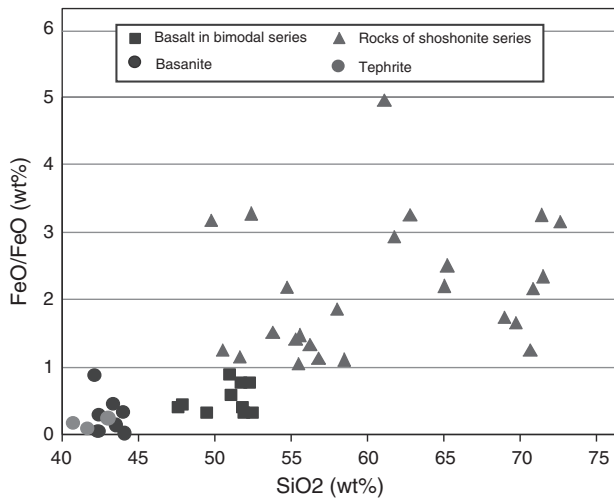


Fig. 5. Oxidation ratios of analyzed volcanic rocks in a $\text{Fe}_2\text{O}_3/\text{FeO}$ – SiO_2 plot. Notice that samples from the shoshonite series rocks are plotted above $\text{Fe}_2\text{O}_3/\text{FeO} = 1$.

Filippova, 1990; Makhbadar and Delgertsogt, 1990) indicate that the occurrence of Cretaceous volcanic rocks in eastern Mongolia. This finding is consistent with the presence of Jurassic and Cretaceous volcanic rocks in the extensional Hailaer Basin and the Greater Xing'an Mountains in northeast China. The volcanic rocks in the basin are rhyolite, latite, trachyte, and andesite that yield U–Pb zircon ages of 111–145 Ma (Ge et al., 2001; J.H. Zhang et al., 2008 L.C. Zhang et al., 2008; Li et al., 2010; Zhao et al., 2013). The volcanic rocks from the same basin also yield $^{40}\text{Ar}/^{39}\text{Ar}$ plateau ages of 121–124 Ma (Wang et al., 2006). All of the age data clearly show that the Early Cretaceous volcanism was intense and widespread in eastern Mongolia and adjacent China.

6.1. Cretaceous volcanism in a regional context

In order to place the Cretaceous occurrence of eastern Mongolian volcanism in a regional context, we briefly outline the tectonic history of northeast Asia since the latest Paleozoic. It is generally agreed that the Paleo-Asian Oceans were closed progressive from west to east from the Permian to the latest Jurassic (e.g., Yin and Nie, 1996). Subduction of the Paleo-Pacific and Pacific plates began in the Early Cretaceous and was expressed by the construction of a continental arc (e.g., Wang and Mo, 1995; Meng and Zhou, 1996; Maruyama et al., 1997; Liu et al., 2001; Taira, 2001). This arc migrates to the a series of island arcs

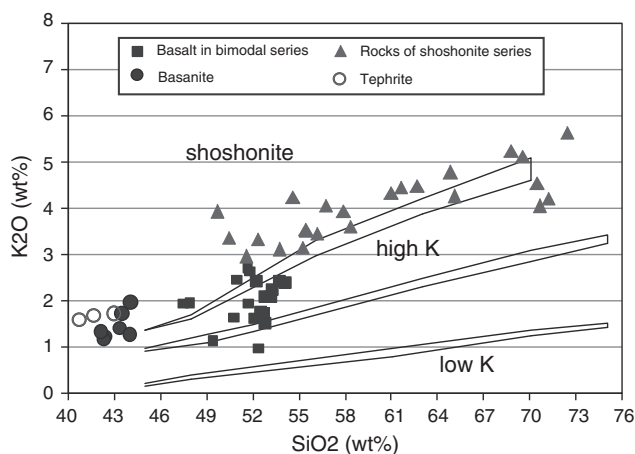


Fig. 6. Classification of volcanic rocks based on K_2O – SiO_2 plot following Peccerillo and Taylor (1976) and Le Maitre et al. (1989).

rifted away from the continental margin of Asia since the Oligo-Miocene due to the opening of the Sea of Japan either by collision-induced lateral extrusion (Jolivet et al., 1994) or back-arc extension (Otofujii and Matsuda, 1983, 1984; Horikoshi, 1990).

6.2. Geochemistry of volcanic rocks from eastern Mongolia and tectonic implications

Our work indicates that Early Cretaceous volcanic rocks in eastern Mongolia, including basaltic rocks from the bimodal series, the basanite series, and most rocks of the shoshonite series, have high Mg#, despite their highly variable SiO_2 contents. Their trace element and Sr–Nd isotopic geochemistry demonstrates that each series involve different mantle sources, magmatic processes and different degrees of crustal contamination.

The basanite series have the highest Mg# (up to 0.67) and initial $^{143}\text{Nd}/^{144}\text{Nd}$ ratios (~0.51267) and the lowest SiO_2 contents and lowest initial $^{87}\text{Sr}/^{86}\text{Sr}$ ratios (~0.70420) in comparison to those from other rock series. This implies that the basanite series may have been derived mainly from a depleted mantle source that was contaminated by crustal material (e.g., Zindler and Hart, 1986; Gribble et al., 1998).

The basaltic rocks from the bimodal series mostly have lower Mg#, lower initial $^{143}\text{Nd}/^{144}\text{Nd}$ ratios, and higher initial $^{87}\text{Sr}/^{86}\text{Sr}$ ratios than those for the basanite series. If the basaltic rocks were also originated from a depleted mantle source, the mantle-derived magma would have contained higher contents of contaminated crustal material than those observed in the basanite series. As the LREE and HREE contents are lower and higher respectively than those for the basanite series, their required enriched mantle source would be chemically different than the depleted mantle source for the basanite series.

The shoshonite series show the largest variation in SiO_2 contents, and most rocks, even including some trachyrhyolite in this series, have high Mg# similar to that measured from the basaltic rocks in the bimodal series. This suggests that the rocks may have been generated from magmatic differentiation. The absarokite and shoshonite have the REE pattern resembling that for the basanite series but differ from that for the basaltic rocks of the bimodal series (Fig. 13). These rocks also have significantly higher initial $^{87}\text{Sr}/^{86}\text{Sr}$ and lower $^{143}\text{Nd}/^{144}\text{Nd}$ ratios than those for the basanite series (Fig. 15). This may be attributed to more contributions of crustal material to the magma source.

It should be noted that all of the three rock series are characterized by high K contents and most of them belong to the shoshonite and high-K calc-alkaline series (Fig. 5). The basaltic rocks have relatively high Mg# and initial $^{143}\text{Nd}/^{144}\text{Nd}$ ratios accompanied by relatively low initial $^{87}\text{Sr}/^{86}\text{Sr}$ ratios, suggesting that all three types of volcanic rocks were derived from a metasomatized mantle source. In detail, the Nb and Ta anomalies (Fig. 14) indicate that the basanite series were derived from a least metasomatized mantle source, the basaltic rocks in the bimodal series were derived from a mantle source metasomatized by crustal material, and the shoshonite series were derived from a most metasomatized source with input from crustal material. Taken together, the Early Cretaceous volcanic rocks in eastern Mongolia were mostly likely derived from heterogeneous mantle sources with a varying degree of contributions from crustal material.

Some workers relate the occurrence of shoshonite and basanite to fractionation of mantle-derived melts during oceanic subduction (Taylor and Karner, 1983; Fryer et al., 1990; Hawkins et al., 1990; Gribble et al., 1996). However, the basaltic rocks from the three rocks series in eastern Mongolia are plotted in within-plate fields AI and AII (Fig. 17A). On the other hand, their Zr/Y ratios are significantly higher than those for within-plate basalts (Fig. 17B). This implies that the Cretaceous volcanic rocks in eastern Mongolia may have been generated by a combined process involving mantle sources generated by both oceanic subduction and within-plate processes such as rising plumes,

Table 3
Chemistry of the basanite and tephrites.

Rock name	Basanite							Tephrite		
Sample N	7/109	7/112	7/114	7/119	7/131	7/1403	7/33	7/113	7/117	7/118
Longitude	115.08.18	115.00.11	114.59.51	115.09.33	114.39.29	114.45.18	114.46.42	114.59.42	115.10.18	115.18.26
Latitude	49.47.00	50.00.03	49.49.33	49.46.29	49.42.44	49.44.04	49.47.06	49.59.18	49.47.10	49.46.13
SiO ₂	42.41	43.5	42.33	43.35	44.06	42.1	44.0	40.72	41.65	43.0
TiO ₂	3.52	2.24	2.21	2.64	2.28	2.1	2.14	2.88	2.54	2.26
Al ₂ O ₃	14.92	13.99	12.77	15.21	15.02	14.32	15.3	15.26	15.2	14.1
Fe ₂ O ₃	2.85	1.30	0.36	3.73	0.18	5.32	2.45	1.51	0.78	1.95
FeO	9.81	9.39	9.0	8.28	9.85	6.04	7.52	8.95	8.75	8.15
MnO	0.17	0.19	0.17	0.28	0.14	0.20	0.20	0.18	0.15	0.18
MgO	7.38	9.02	10.78	8.84	7.93	10.36	8.26	5.27	9.12	8.73
CaO	9.47	8.52	10.12	9.12	11.02	8.37	7.92	10.29	9.12	9.54
Na ₂ O	4.14	5.25	6.33	4.79	4.24	4.92	5.09	5.92	5.34	5.43
K ₂ O	1.22	1.72	1.15	1.4	1.96	1.33	1.27	1.59	1.68	1.72
P ₂ O ₅	0.9	0.86	0.82	0.85	0.53	2.16	2.16	1.27	0.58	0.83
LOI	0.09	2.54	2.95	1.44	2.62	2.41	3.08	5.74	3.22	3.57
Σ	96.88	98.52	98.99	99.93	99.8	99.63	99.39	99.58	97.55	99.46
Fet	12.66	10.69	9.36	12.01	10.03	11.36	9.97	10.46	9.53	10.1
Fet/Mg	1.72	1.19	0.87	1.36	1.26	1.10	1.21	1.98	1.04	1.16
Fe ₂ O ₃ /FeO	0.29	0.14	0.04	0.45	0.02	0.88	0.33	0.17	0.09	0.24
Na + K	5.36	6.97	7.48	6.19	6.2	6.25	6.36	7.51	7.02	7.15
K/Na	0.29	0.33	0.18	0.29	0.46	0.27	0.25	0.27	0.31	0.32
ppm										
Co	32.50	36.40	41.60					30.50	30.30	
Ni	210.0	285.0	300.0					113.0	152.0	
Ga	20.1	20.5	17.7					23.4	18.4	
Rb	42.8	44.7	27.1					47.2	40.4	
Sr	1276.1	1214.5	1364.3					1836	1432.6	
Y	28.7	24.5	23.8					32.7	23.4	
Zr	305.2	312.1	262.2					406.2	280.9	
Nb	90.6	71.63	76.22					128	95.2	
Cs	1.85	1.62	3.37					1.72	2.19	
Ba	977.4	806.1	1126.5					1368.5	1055	
Hf	7.49	7.32	6.49					9.64	7.58	
Ta	6.58	4.74	4.95					8.59	4.43	
Pb	3.06	5.74	5.33					6.86	4.74	
Th	8.24	7.42	6.25					11.35	9.75	
U	2.09	1.76	1.37					2.41	1.83	
La	87.69	72.23	71.25					118.12	86.45	
Ce	165.2	135.4	134.54					217.4	160.7	
Pr	18.76	15.82	16.10					25.51	18.23	
Nd	62.88	55.57	56.89					88.51	59.94	
Sm	10.9	10.09	10.34					15.17	11.2	
Eu	3.04	2.85	2.87					4.12	2.96	
Gd	9.11	8.36	8.44					12.11	8.84	
Tb	1.23	1.11	1.09					1.57	1.07	
Dy	5.97	5.47	5.22					7.38	5.67	
Ho	1.09	0.99	0.95					1.31	1.05	
Er	2.68	2.51	2.46					3.34	2.59	
Tm	0.37	0.35	0.33					0.46	0.36	
Yb	2.25	2.13	2.07					2.83	2.20	
Lu	0.33	0.31	0.29					0.41	0.32	

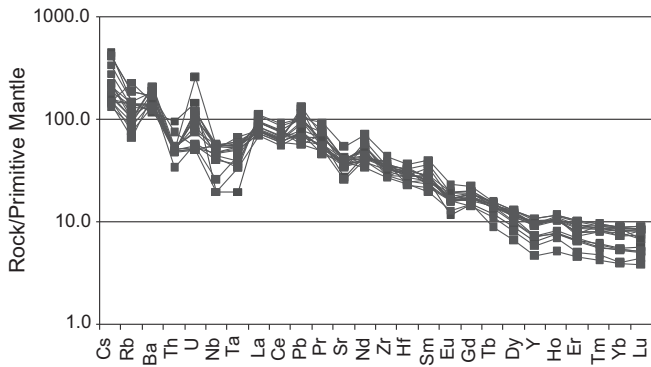


Fig. 7. Trace element contents normalized to primitive mantle value for samples from bimodal-series rocks following Sun and McDonough (1989). Notice that Rb, Ba, Th, U, and Ce display positive anomalies whereas Nb and Ta show negative anomalies.

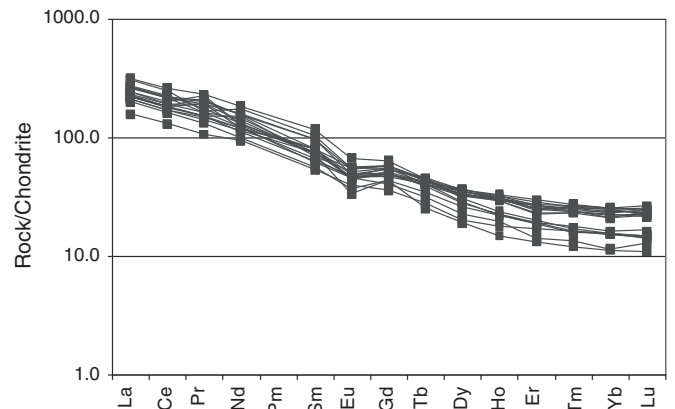


Fig. 8. Chondrite-normalized REE plot for samples from the bimodal series rocks. Notice that the REE distribution diagram displays a slightly negative anomaly of Eu.

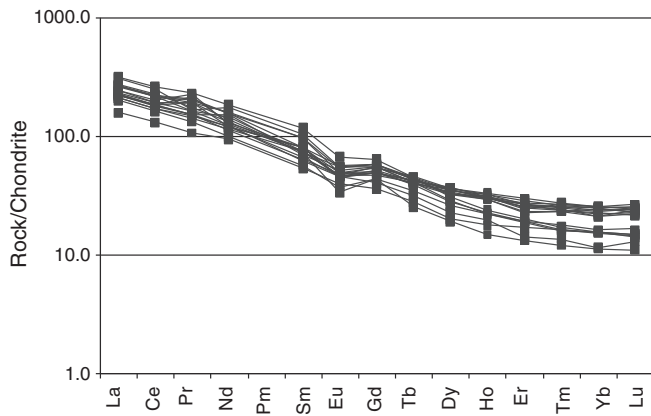


Fig. 9. Chondrite-normalized REE plot for samples from the shoshonite series rocks. Notice that the distribution pattern displays a slightly negative Eu anomaly for mafic rocks from the shoshonite series. In contrast, Eu is strongly negative for intermediate and felsic rocks of the shoshonite series.

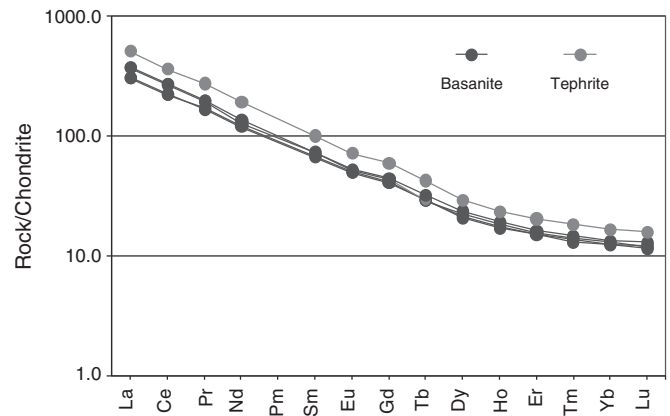


Fig. 11. Chondrite-normalized REE plot for basanite and tephrite samples.

delamination of mantle lithosphere, and lithospheric avalanche (see detailed discussion below).

6.3. Age pattern and eastern delamination across eastern Mongolia and NE China

The newly obtained ages of volcanic rocks from eastern Mongolia provide a test for the existing tectonic models for Cretaceous volcanism in eastern Mongolia and NE China. Based on a systematic dating of volcanic rocks and a synthesis of regional tectonic events, Wang et al. (2006) noted that the onset of Mesozoic volcanism in the Greater Xing'an Mountains of NE China started first at about 160 Ma in the east; Mesozoic volcanism swept westward till about 110 Ma across NE China. This proposed age pattern is consistent with other studies that show Jurassic volcanism occurred in the Greater Xing'an region and southeast Mongolia in the Middle and Late Jurassic (e.g., Graham et al., 2001; J.H. Zhang et al., 2008; Zhang et al., 2010). Based on the above observations, Wang et al. (2006) suggested that the westward migration of volcanism across southeastern Mongolia and NE China was a result of westward delamination of an early thickened mantle lithosphere from below; the thickened mantle lithosphere was created by the closure of the Mongolo-Okhotsk Ocean, the final trace of the much larger Paleo-Asia oceans. The timing of the ocean closure at ~160 Ma in the Jurassic in this region (Yin and Nie, 1996) fits approximately to the proposed timing of initial volcanism in the area as dated by Wang et al. (2006). A prediction of the Wang et al. (2006) model is that

volcanism in eastern Mongolia, where the final closure site of the Mongol-Okhotsk Ocean is located, should have started at about 160 Ma immediately after the closure of the Mongol-Okhotsk Ocean. Our newly acquired dates for two volcanic samples yield ages of 110–104 Ma and previous K–Ar and Rb–Sr dating of other volcanic rocks in our study areas yield ages of ~120 Ma (Solovyev et al., 1977a, b; Frikh-Har and Luchitskaya, 1978; Shuvalov, 1988). If these ages represent the true duration of volcanism in eastern Mongolia, then the age pattern across eastern Mongolia and NE China would be inconsistent with the Wang et al. (2006) model. The limitation of this conclusion is that the number of dated samples is too few to be statistically significant. In addition, we note that the area directly south and southwest of our sample sites exposes Middle and Late Jurassic volcanic rocks (Graham et al., 2001). It is currently unclear if these older volcanic rocks are also present in our study area due to the reconnaissance nature of our work.

6.4. Tectonic models and future studies

The Cretaceous riebeckite rhyolites in the southern Greater Xing'an region of NE China may have been erupted in an extensional setting after the closure of the Mongol-Okhotsk Ocean. This is evident from the presence of Cretaceous volcanic rocks within coeval extensional basins (e.g., Zhao et al., 2013) and occurrence of A-type granite and dolerite dike swarms (Wu et al., 2005a,b). This interpretation also is consistent with the development of extensional metamorphic core

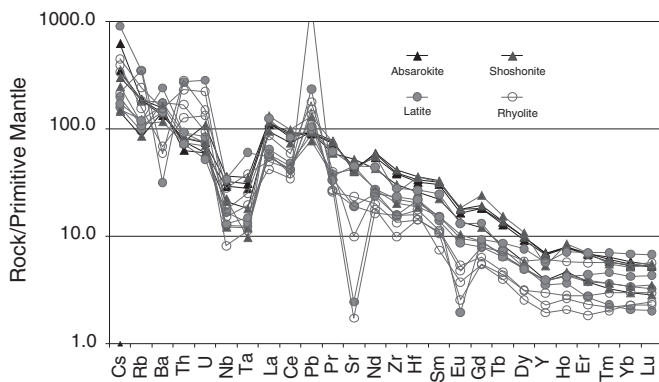


Fig. 10. Trace element contents normalized to primitive mantle value for samples from the shoshonite series rocks. Notice that Rb, Ba, Th, La, and Ce display positive anomalies whereas Nb and Ta display strongly negative anomalies.

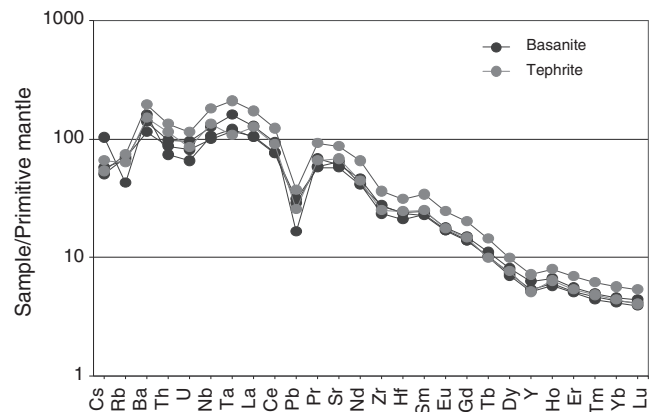


Fig. 12. Trace element contents normalized to primitive mantle value for basanite and tephrite samples.

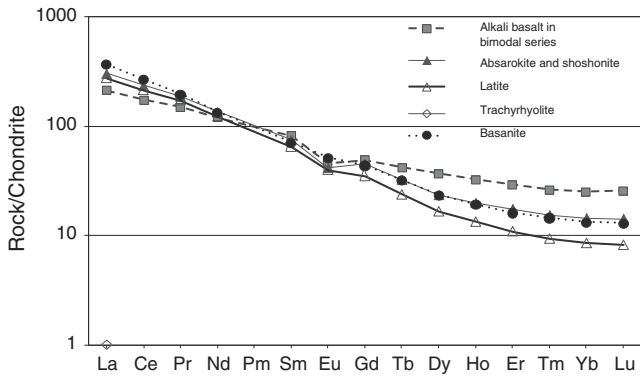


Fig. 13. Summary plot of chondrite-normalized REE patterns for samples from bimodal-series, shoshonite-series and basanite rocks.

complexes across northeastern Asia at this time (e.g., Davis et al., 1996, 1998, 2001; Wang et al., 2011).

In the southern segment of the eastern margin of Asia, the Cretaceous volcanic rocks are well developed in Southeast China and erupted during 146–97 Ma, coeval with A-type granites, implying an extensional environment (T.-D. Li, 2000; X.H. Li, 2000). These high-K calc-alkaline volcanic rocks show the geochemical features similar to those formed in continental back-arc and post-collisional extensional settings, and the eruption centers are spatially associated with extensional basins and basin-bounding normal faults due to lithospheric extension (T.-D. Li, 2000; X.H. Li, 2000). The Cretaceous tholeiitic basalts in the interior of the South China Craton interlayer with red beds in extensional basins and may have resulted from the interaction of back-arc extension and upper-mantle melting (Zhou et al., 2006).

The great distance (>500 km) from the active arc at the time of Cretaceous volcanism in eastern Mongolia places the volcanic field in a back-arc setting (Fig. 18). Such a setting is compatible with the occurrence of shoshonite and basanite, because these rocks are commonly associated with back-arc extension (Taylor and Karner, 1983; Hawkins et al., 1990; Peate et al., 1997; Sinton et al., 2003; Taylor and Martinez, 2003; Gill et al., 2004; Kay and Copeland, 2006). In a back-arc setting, a few factors may influence petrologic and geochemical signatures of the spatially related volcanism. They include (1) inputs of recycled continental components derived from seawater and subducted sediments, (2) magnitude of back-arc extension, (3) temporal evolution of the back-arc basin, (4) mantle flow patterns below the arc, and (5) contamination of crustal material due to magmatic assimilation of pre-existing wall rock (Mackenzie and Chapell, 1972; Hawkins and Melchior, 1985; Volpe et al., 1987; Hawkins et al., 1990; Stern et al., 1990; Peate et al., 1997; Gribble et al., 1998; Turner and Hawkesworth, 1998; Martinez

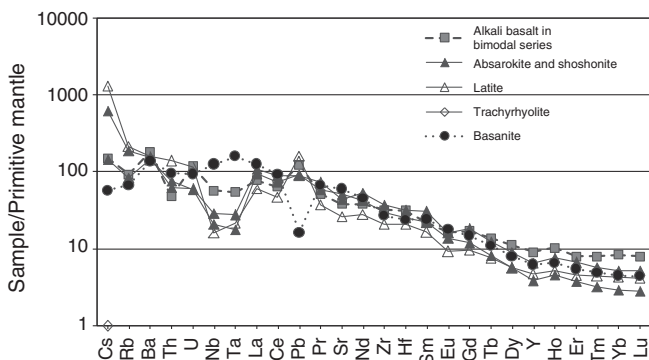


Fig. 14. Summary plot of trace-element contents normalized to the primitive mantle value for samples from the bimodal-series, shoshonite-series, and basanite rocks.

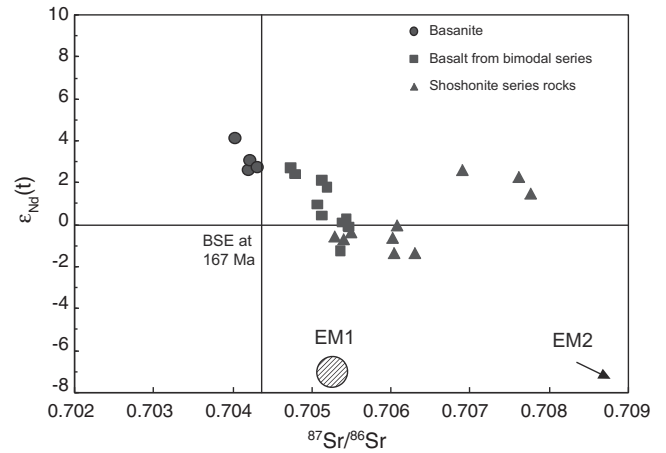


Fig. 15. Nd–Sr plot for basanite, bimodal series rocks, and shoshonite series rocks.

and Taylor, 2003, 2006). These complications make it difficult to derive a unique interpretation without consulting with local and regional geologic contexts.

The young ages of Cretaceous volcanism across eastern Mongolia and NE China obtained from this study and the early work contradict the prediction of the Wang et al. (2006) model. There are two possible explanations for this age discrepancy. First, the westward delamination of the thickened lithosphere from the Mongol–Okhotsk suture may have

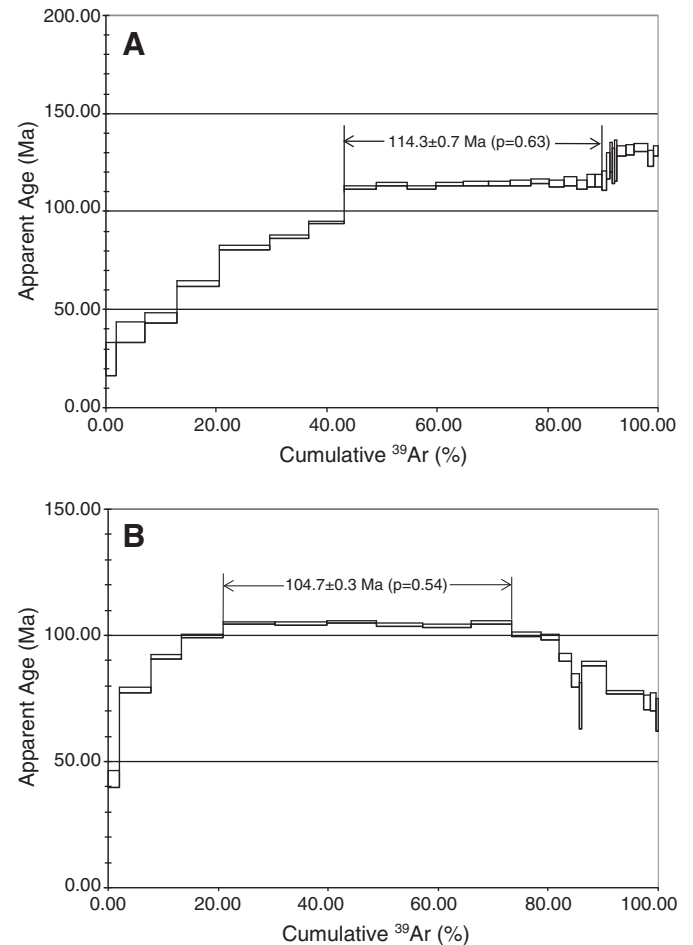


Fig. 16. (A) Whole-rock $^{40}\text{Ar}/^{39}\text{Ar}$ age spectrum from a shoshonite sample in the Tsaganjelger area. (B) Whole-rock $^{40}\text{Ar}/^{39}\text{Ar}$ age spectrum from a basanite sample in the Dych Gol area.

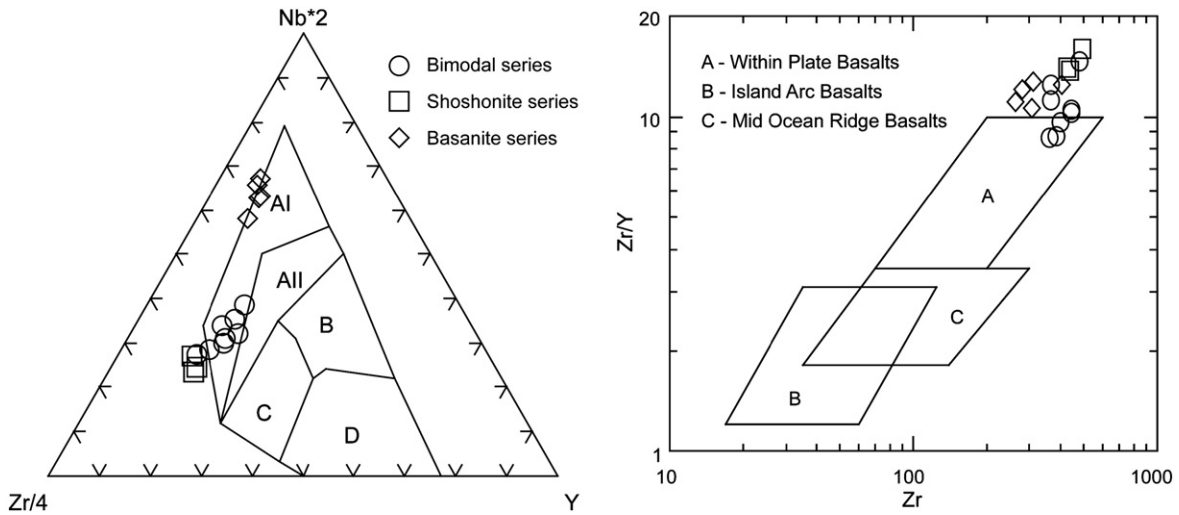


Fig. 17. A Th–Hf/3–Nb/16 plot after Wood (1980). Region B, tholeiitic basalt from mid-ocean ridge (MORB) and within-plate setting (WPB; region D, convergent plate-margin basalt and its derivatives; C, alkaline within-plate basalt (WPPB).

caused eastward propagation of the volcanic front but the process did not shut down volcanism completely trailing behind the volcanic front. The younger volcanism in eastern Mongolia could be a result of this process. However, this explanation would require that volcanism in eastern Mongolia had started at about 160 Ma for which we currently do not have any evidence to support it. The second explanation for the apparent age discrepancy between volcanism in eastern Mongolia and prediction by the Wang et al. (2006) model is suggested below. It is

likely that the location of initial delamination as proposed by Wang et al. (2006) occurred between our study area and the western edge of the Great Xing'an volcanic field in NE China. The previously thickened mantle lithosphere was delaminated into two slabs and propagated to both the east and west. This process caused two volcanic fronts moving in the opposite direction (Fig. 19). In this model, the younger volcanic rocks found in eastern Mongolia had resulted from westward delamination of the previously thickened mantle lithosphere, whereas the

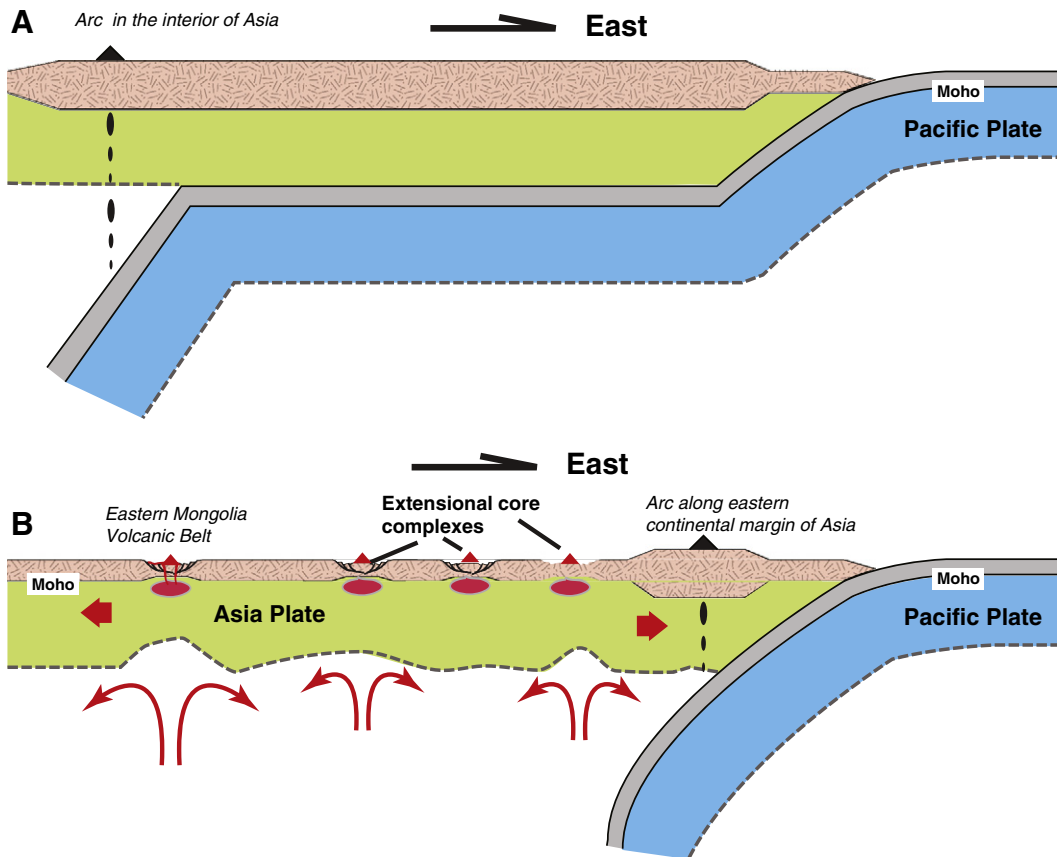


Fig. 18. Flat subduction to broad back-arc extension and volcanism. (A) The Pacific slab may have extended far inland in the Middle and Late Jurassic, which explains the early occurrence of volcanism in eastern Mongolia and westernmost Greater Xing'an volcanic field in NE China. (B) Rapid slab retreat to the west may explain the observed westward migration pattern of volcanism across NE China.

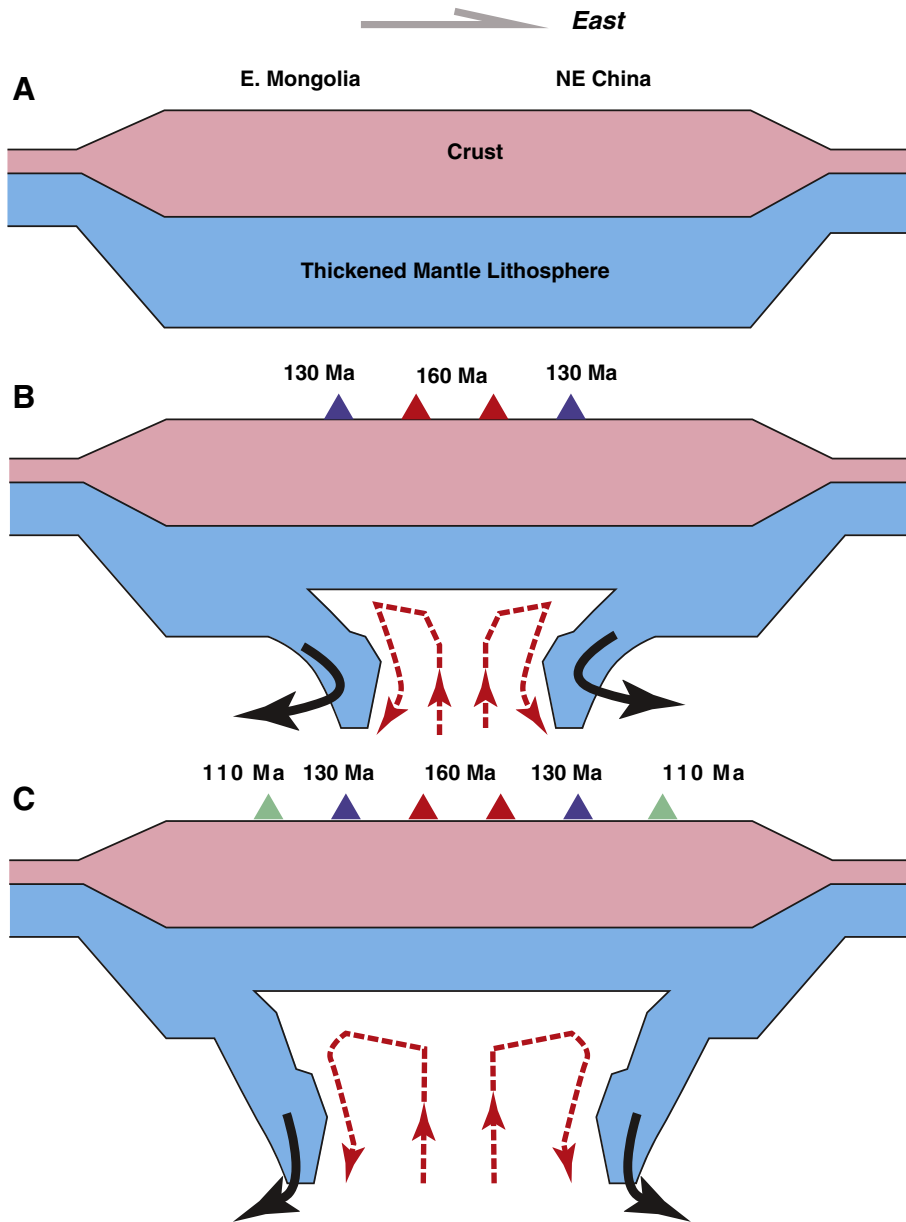


Fig. 19. A possible model to explain the age pattern of Mesozoic volcanism across eastern Mongolia and NE China. (A) Thickened mantle lithosphere was created during the closure of the Mongol-Okhotsk Ocean at about 160 Ma. (B) Partial delamination of the thickened mantle lithosphere occurred immediately after the ocean closure to the west and east, leading to mantle upwelling below and volcanism at the surface. (C) Bi-directional propagation of delamination caused progressive younging of the volcanic front to the west and east, reaching eastern Mongolia where our study was conducted at about 110 Ma.

eastward development of the Greater Xing'an volcanic field was induced by delamination of the eastern limb of the torn mantle lithosphere (Fig. 19).

The bi-directional delamination model is site-specific and explains well the *currently known* temporal development of Mesozoic volcanism in eastern Mongolia. Another possible site-specific model is that Cretaceous volcanism in eastern Mongolia was induced by mantle avalanche (Fig. 20). As pointed out by Schubert and Tackley (1995) mantle avalanches can produce thermal effects similar to activities of rising mantle plumes by bring anomalously hot mantle materials to the base of the lithosphere. According to their model, an avalanche takes place where a large amount of cold materials from subducted slabs is piled up at the 670 km phase boundary. When these cold materials rapidly were flush down into the lower mantle and are replaced by hotter mantle materials from below, melting cold have occurred in the upper mantle. Applying the concept of this model, we envision that the final

suturing of the Paleo-Asia oceans may have left a thick pile of cold subducted materials at the 670 km phase boundary below the orogenic belt (Fig. 20A). Thermal perturbation of the upper mantle via subduction of the Pacific plate may have increased the mantle temperature and thus lowered the viscosity of the upper mantle. This in turn favored rapid sinking of the cold pile of lithosphere through the 670 km phase boundary (e.g., Tackley et al., 1993; Tackley, 2000). Finally, mantle materials filling the gap of the slab pile caused upwelling and thus decompressional melting (Fig. 20B). Although only one blob is shown in the figure, it is possible that several piles of cold mantle materials were flushed down at different locations below a vast region of eastern Asia, causing diachronous upwelling of mantle and melting and an irregular age pattern of volcanism. The advantage of this model is its ability to relate the early tectonic history of eastern Mongolia with the subsequent Cretaceous volcanism. However, testing this model is challenging as it requires careful restoration of the position and history

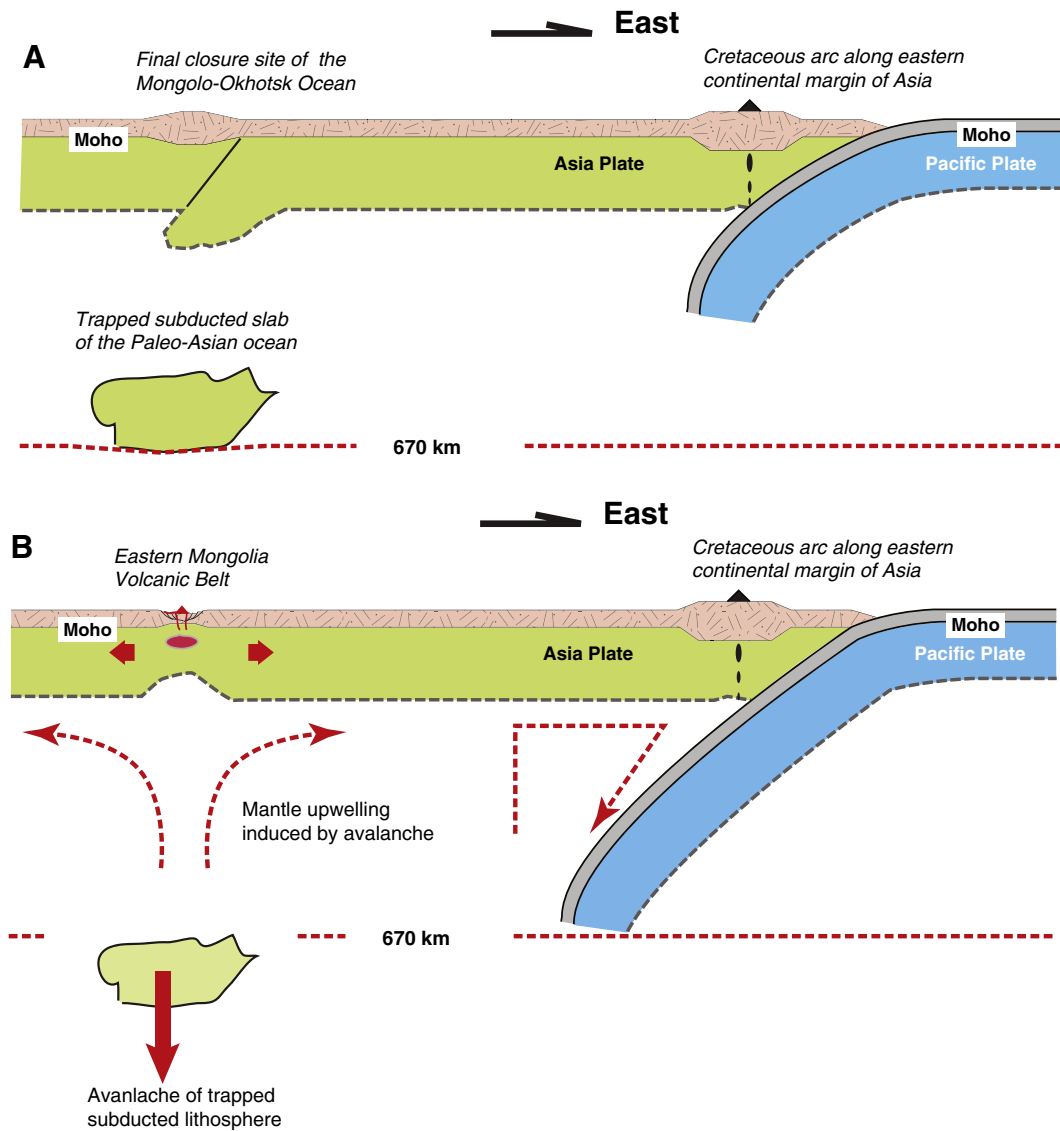


Fig. 20. (A) A thick pile of subducted oceanic slabs from the Paleo-Asia oceans was trapped at the top of the endothermic phase boundary at 670 km. The cold temperature in the upper mantle due to addition of the subducted slab prevented the slab to sink through the phase boundary. (B) The initiation of the Pacific subduction may have caused a thermal perturbation, raising the temperature and thus reducing the viscosity of the upper mantle via upward mantle generated by the subduction.

of subducted Paleo-Asian oceanic slabs with the highly interpretative tomographic images (e.g., Van der Voo et al., 1999; Lebedev et al., 2006; Zhao et al., 2009).

As indicated by the elemental and isotopic data discussed above, Cretaceous volcanism in eastern Mongolia could have been induced by mantle upwelling related to back-arc extension within a continental lithosphere. This process could explain the complex source characteristics and contamination of continental materials in the final products of the erupted lava. Thus, Cretaceous volcanism in eastern Mongolia could have occurred in a rift zone in the back arc region of the westward subduction of the Pacific plate (Fig. 18). In contrast to the site-specific models shown in Figs. 19 and 20, this regional model explains the overall Cretaceous volcanism across the eastern margin of Asia that is parallel to the Pacific subduction zone (e.g., Li, 2000; Wu et al., 2005a,b). It also explains the close association between Cretaceous detachment-fault terranes and volcanism (Davis et al., 1996, 1998, 2001; Wu et al., 2005b; Wang et al., 2011, 2012). It is possible that the wide extension and volcanism across eastern Asia including eastern Mongolia was induced by flat subduction of the Pacific plate followed by rapid steepening towards the trend eastward in the Mesozoic as

envisioned by Zhao et al. (2009). This scenario implies that the upwelling of the asthenosphere mantle below Asian lithosphere in the back-arc region is not concentrated at one narrow zone but rather distributed widely over a large area across eastern Asia (>1000 km from the trench to the continental interior). This process may be similar to the development of the Laramide orogeny in the North American Cordillera during the flat subduction of the Farellon plate; it was followed by a rapid retreat of the slab towards the trench and widely developed extensional core complexes across the western North America (e.g., Coney and Harms, 1984; Yin, 1989). It is possible that the collapsed flat slabs were broken into small pieces and their downward sinking produced small scale convection cells that led to upper-mantle melting. A similar model of slab-fragment sinking was proposed by Yin (2010) to explain a wide occurrence of Cenozoic intra-plate volcanism across Asia. Our slab-retreat model is somewhat similar to the model of Li and Li (2007) for the development of a wide Mesozoic extensional orogen in South China. As shown in Fig. 18, the Pacific slab may have extended far inland in the Middle and Late Jurassic, which explains the early occurrence of volcanism in eastern Mongolia (Graham et al., 2001) and the westernmost Greater Xing'an volcanic

field in NE China (Wang et al., 2006). Rapid slab retreat to the west from the Late Jurassic to the Early Cretaceous may explain the observed westward migration of volcanism across NE China (Wang et al., 2006).

A major shortcoming of our work that hinders an effective test of the above competing models is the lack of detailed geologic surveys in the field over our sampling sites. As a result, it is currently unclear the exact stratigraphic positions of our samples and the true statistical significance of the limited age data from the region. A systematic mapping and sampling across eastern Mongolia and far-east Russia should be a priority in future investigations on the origin of Cretaceous volcanism in this vast area.

7. Conclusions

Cretaceous volcanism occurred over a wide region of eastern Asia from Siberia in the north to SE Asia in the south. Hypotheses for its occurrence include intra-continental rifting, formation of a continental arc, rising plume, and delamination of previously thickened mantle lithosphere. A major difficulty in testing the above competing models is the lack of modern geologic studies of volcanic rocks in eastern Mongolia and Siberia. In this study, we investigate this issue by examining the timing and geochemistry of Cretaceous volcanic rocks in eastern Mongolia. Our work in conjunction with early studies reveals the occurrences of three types of volcanic rocks in eastern Mongolia between 120 Ma and 104 Ma: (1) a bimodal series, (2) a shoshonite series, and (3) a basanite series. Geochemical analysis of the volcanic rocks indicates a highly heterogeneous source characterized a mixture of depleted, enriched and metasomatized mantle. When combined with constraints on the timing, tectonic history, and tectonic setting of the region where the volcanic rocks are examined, we derived three possible models for the occurrence of Cretaceous volcanism in eastern Mongolia: (1) bi-directional delamination of a previously thickened mantle lithosphere, (2) back-arc extension due to collapse of a flat subduction slab, and (3) mantle avalanche a thick pile of trapped cold mantle materials from the subducted Paleo-Asian oceanic plates across the 670-km endothermic phase transition. Differentiating the above competing models is difficult at the present due to the lack of detailed geologic information on Cretaceous volcanic rocks across the vast region of eastern Mongolia and far-east Siberia. A careful restoration of the position and history of the past subducted slabs of the Paleo-Asian oceans in the mantle in the future may help differentiate the above competing models.

Acknowledgment

We thank the three anonymous reviewers for their critical yet constructive comments. We also thank the journal editor for his suggestions in improving the original draft of the paper. An Yin's research in Asia is supported by grants from the Tectonics Program of U.S. National Science Foundation.

Appendix A. Supplementary data

Supplementary data to this article can be found online at <http://dx.doi.org/10.1016/j.gr.2013.10.001>.

References

- Badarch, G., Cunningham, W.D., Windley, B.F., 2002. A new terrane subdivision for Mongolia: implications for the Phanerozoic crustal growth of Central Asia. *Journal of Asian Earth Sciences* 21, 87–110.
- Baljinnyam, V., Batjargal, S., Batulzii, D., Lhamsuren, J., 1989. The volcanic and plutonic rocks of Tsav in Eastern Mongolia represent a shoshonite series rocks. In: Gerel, O., Ivanov, A.N. (Eds.), *Problems Geology and Mineral Resources in Mongolia*, pp. 34–45 (Mongolian Geological Survey, Ulaanbaatar).
- Briggs, S.M., Yin, A., Manning, C.E., Chen, Z.L., Wang, X.F., Grove, M., 2007. Late Paleozoic tectonic history of the Ertix Fault in the Chinese Altai and its implications for the development of the central Asian orogenic system. *Geological Society of America Bulletin* 119, 944–960.
- Briggs, S.M., Yin, A., Manning, C.E., Chen, Z.L., Wang, X.F., 2009. Tectonic development of the southern Chinese Altai Range as determined by structural geology, thermobarometry, ⁴⁰Ar/³⁹Ar thermochronology, and Th/Pb ion-microprobe monazite geochronology. *Geological Society of America Bulletin* 121, 1381–1393. <http://dx.doi.org/10.1130/B26344.1>.
- Coney, P.J., Harms, T.A., 1984. Cordilleran metamorphic core complexes: Cenozoic extensional relics of Mesozoic compression. *Geology* 12, 550–554.
- Dash, B., 1996. Petrology and geochemistry of latites in northeastern Mongolia (with an example from the Tsav area) (Summary of the Ph.D. thesis. Mongolia University of Science and Technology, Ulaanbaatar. 25 pp.).
- Davis, G.A., Qian, X., Zheng, Y.D., Tong, H.M., Yu, H., Gehrels, G., Shafiqullah, M., Fryxell, J., 1996. Mesozoic deformation and plutonism in the Yunneng Shan: a metamorphic core complex north of Beijing, China. In: Yin, A., Harrison, T.M. (Eds.), *The Tectonic Evolution of Asia*. Cambridge University Press, Cambridge, pp. 253–280.
- Davis, G.A., Wang, C., Zheng, Y.D., Zhang, J.J., Zhang, C.H., Gehrels, G.E., 1998. The enigmatic Yinshan fold-and-thrust belt of northern China: new views on its intraplate contractional styles. *Geology* 26, 43–46.
- Davis, G.A., Zheng, Y.D., Wang, C., Darby, B.J., Zhang, C.H., Gehrels, G., 2001. Mesozoic tectonic evolution of the Yanshan fold and thrust belt, with emphasis on Hebei and Liaoning provinces, Northern China. *Geological Society of America Memoir* 2001, 171–197.
- Deino, A.L., 2001. *Users Manual for Mass Spectrometers*, v. 5.02. Berkeley Geochronology Center Special Publication, 1A (119 pp.).
- Dobrolubov, B.A., Flippova, I.B., 1990. The geology, rock chemistry, and fluorine mineralizations of north west part, Eastern Mongolian rift belt. In: Marinov, N.A. (Ed.), *Geology and Mineral Resources of Mongolia*, 3. Nedra Press, Moscow, pp. 108–123.
- Fan, W.M., Guo, F., Wang, Y.J., Lin, G., 2003. Late Mesozoic calc-alkaline volcanism of post-orogenic extension in the northern Da Xing'an Mountains, northeastern China. *Journal of Volcanology and Geothermal Research* 121, 115–135.
- Filippova, I.B., Suetenko, O.D., Khasin, P.A., 1984. Mesozoic geodynamic setting and some metallogeny features of eastern Mongolia. In: Marinov, N.A. (Ed.), 2. *Geology and mineral resources of Mongolia*, 2. Nedra Press, Moscow, pp. 27–46.
- Frikh-Har, D.L., Luchitskaya, A.I., 1978. Late Mesozoic volcanites and associated hypabyssal intrusives of Mongolia. *Nauka, Moscow* (168 pp.).
- Fryer, P., Taylor, B., Langmuir, C.H., Hochstaedter, A.G., 1990. Petrology and geochemistry of lavas from the Sumisu and Torishima backarc rifts. *Earth and Planetary Science Letters* 100, 161–178.
- Gantumur, K., 2005. *Geological characteristics and genesis of the Tsav Ag–Pb–Zn deposit, Eastern Mongolia* (Summary of the Ph.D. thesis, Mongolia University of Science and Technology, Ulaanbaatar. 21 pp.).
- Ge, W.C., Li, X.H., Lin, Q., Sun, D.Y., Wu, F.Y., Yun, S.H., 2001. Geochemistry of early Cretaceous alkaline rhyolites Hulun Lake, Daxinganling and its tectonic implications. *Chinese Journal of Geology* 36, 176–183 (in Chinese with English abstract).
- Gill, R.C.O., Aparicio, A., Azzouzi, M.E., Hernandez, J., Thirlwall, M.F., Bourgois, J., Marriner, G.F., 2004. Depleted arc volcanism in the Alboran Sea and shoshonitic volcanism in Morocco: geochemical and isotopic constraints on Neogene tectonic processes. *Lithos* 78, 363–388.
- Graham, S.A., Hendrix, M.S., Johnson, C.L., Badamgarav, D., Badarch, G., Amory, J., Porter, M., Barsbold, R., Webb, L.E., Hacker, B.R., 2001. Sedimentary record and tectonic implications of Mesozoic rifting in southeast Mongolia. *Geological Society of America Bulletin* 113 (12), 1560–1579.
- Gribble, R.F., Stern, R.J., Bloomer, S.H., Stüben, D., O'Hearn, T., Newman, S., 1996. MORB mantle and subduction components interact to generate basalts in the Southern Mariana Trough back-arc basin. *Geochimica et Cosmochimica Acta* 60, 2153–2166.
- Gribble, R.F., Stern, R.J., Newman, S., Blommer, S.H., O'Hearn, T., 1998. Chemical and isotopic composition of lavas from the northern Mariana Trough: implications for magmagenesis in back-arc basin. *Journal of Petrology* 39, 125–154.
- Hawkins, J.W., Melchior, J.T., 1985. Petrology of Mariana Trough and Lau Basin basalts. *Journal of Geophysical Research* 90, 11431–11468.
- Hawkins, J.W., Lonsdale, P.F., MacDougall, J.D., Volpe, A.M., 1990. Petrology of the axial ridge of the Mariana Trough backarc spreading center. *Earth and Planetary Science Letters* 100, 226–250.
- Horikoshi, E., 1990. Opening of the Sea of Japan and Kuro deposit formation. *Mineral Deposits* 25, 140–145.
- Jahn, B.M., 2004. The Central Asian Orogenic Belt and growth of the continental crust in the Phanerozoic. In: Malpas, J., Fletcher, C.J.N., Ali, J.R., Aitchison, J.C. (Eds.), *Aspects of the tectonic evolution of China*. The Geological Society of London, pp. 73–100.
- Jakes, P., White, A.J.R., 1972. Major and trace element abundances in volcanic rocks of orogenic areas. *Bulletin Geological Society of America* 83, 29–40.
- Jolivet, L., Tamaki, K., Fournier, M., 1994. Japan Sea, opening history and mechanism: a synthesis. *Journal of Geophysical Research* 99, 22237–22259.
- Kay, S.M., Copeland, P., 2006. Early to middle Miocene backarc magmas of the Neuque'n basin: geochemical consequences of slab shallowing and the westward drift of South America. In: Kay, S.M., Ramos, V. (Eds.), *Evolution of an Andean Margin*. In *A Tectonic and Magmatic View from the Andes to the Neuque'n Basin* (35–39S lat.). *Spec. Pap. Geol. Soc. Am.*, 407, pp. 185–213.
- Kelty, T.K., Yin, A., Dash, B., Gehrels, G.E., Ribeiro, A.E., 2008. Detrital –zircon geochronology of Paleozoic sedimentary rocks in the Hangay–Hentey basin, north central Mongolia: implications for the tectonic evolution of the Mongol–Okhotsk Ocean in central Asia. *Tectonophysics* 451, 290–311.
- Kovalenko, V.I., Yarmolyuk, V.V., 1990. Evolution of magmatism in the structures of Mongolia. Evolution of geological processes and metallogeneses of Mongolia. *Nauka Press, Moscow*, pp. 23–55.
- Kröner, A., Kovach, V., Belousova, E., Hegner, E., Armstrong, R., Dolgoplova, A., Seltmann, R., Alexeiev, D.V., Hoffmann, J.E., Wong, J., Sun, M., Cai, K., Wang, T., Tong, Y., Wilde, S.A., Degtyarev, K.E., Ryttsk, E., 2014. Reassessment of continental growth during the

- accretionary history of the Central Asian Orogenic Belt. *Gondwana Research* 25 (1), 103–125.
- Le Maître, R.W., Bateman, P., Dudek, A., Keller, J., Lameyre Le Bas, M.J., Sabine, R.A., Schmid, R., Sorensen, N., Streckeisen, A., Wolley, A.R., Zanettin, B., 1989. *A Classification of Igneous Rocks and Glossary of Terms*. Blackwell, Oxford.
- Lebedev, S., Meier, T., van der Hilst, R., 2006. Asthenospheric flow and origin of volcanism in the Baikal Rift area. *Earth and Planetary Science Letters* 249, 415–424. <http://dx.doi.org/10.1016/j.epsl.2006.07.007>.
- Li, X.H., 2000. Cretaceous magmatism and lithospheric extension in Southeast China. *Journal of Asian Earth Sciences* 18, 293–305.
- Li, T.-D. (chief editor), 2000. *Geologic Map of Asia and Eurasia*, 1:5,000,000.
- Li, Z.X., Li, X.H., 2007. Formation of the 1300-km-wide intracontinental orogen and postorogenic magmatic province in Mesozoic South China: a flat-slab subduction model. *Geology* 35, 179–182.
- Li, P.P., Ge, W.C., Zhang, Y.L., 2010. Division of volcanic strata in the northwestern part of Hailar basin: evidence from zircon U–Pb dating. *Acta Petrologica Sinica* 26, 2482–2494 (in Chinese with English abstract).
- Liu, J.Q., Han, J.T., Fyfe, W.S., 2001. Cenozoic episodic volcanism and continental rifting in northeast China and possible link to Japan Sea development as revealed from K–Ar geochronology. *Tectonophysics* 339, 385–401.
- Mackenzie, D.E., Chapell, B.W., 1972. Shoshonitic and calc alkaline lavas from the Highlands of Papua New Guinea. *Contributions to Mineralogy and Petrology* 35, 50–62.
- Makhbadar, T.S., Delgertsogt, B., 1990. Geological map Central and Eastern Mongolia, scale 1:500000 with brief introduction. Ulaanbaatar.
- Martinez, F., Taylor, B., 2003. Controls on back-arc crustal accretion: insights from the Lau, Manus and Mariana basins. In: Larter, R.D., Leat, P.T. (Eds.), *Intra-Oceanic Subduction Systems: Tectonic and Magmatic Processes*. Geological Society of London Special Publications, 219, pp. 19–54.
- Martinez, F., Taylor, B., 2006. Modes of crustal accretion in back-arc basins: Inferences from the Lau Basin. In: Christie, D.M., Fisher, C.R., Lee, S.-M., Givens, S. (Eds.), *Back-Arc Spreading Systems: Geological, Biological, Chemical and Physical Interactions*. American Geophysical Union, Washington, DC, pp. 5–30.
- Maruyama, S., Isozaki, Y., Kimura, G., Terabayashi, M., 1997. Paleogeographic maps of the Japanese Islands: plate tectonic synthesis from 750 Ma to the present. *Island Arc* 6, 121–142.
- Meng, Q.L., Zhou, Y.X., 1996. The formation and evolution of magma for J2-K1 volcanic-intrusive complex in Eastern Yunnan, Jilin Province. *Acta Petrologica et Mineralogica* 15, 30–39 (in Chinese with English abstract).
- Morrison, G.W., 1980. Characteristics and tectonic setting of the shoshonite rock association. *Lithos* 13, 97–108.
- Nagibna, M.S., 1975. Mesozoic revivification structures. In: Yanshin, A.L. (Ed.), *Mesozoic–Cenozoic tectonics and the Magmatism of Mongolia*. Nauka Press, Moscow, pp. 18–103.
- Otofujii, Y.-I., Matsuda, T., 1983. Paleomagnetic evidence for the clockwise rotation of Southwest Japan. *Earth and Planetary Science Letters* 62, 349–359.
- Otofujii, Y.-I., Matsuda, T., 1984. Timing of rotational motion of Southwest Japan inferred from paleomagnetism. *Earth and Planetary Science Letters* 70, 373–382.
- Peate, D.W., Pearce, J.A., Hawkesworth, C.J., Colley, H., Edwards, C.M.H., Hirose, K., 1997. Geochemical variations in Vanuatu lavas; the role of subducted material and a variable mantle wedge composition. *Journal of Petrology* 38, 1331–1358.
- Pecceirillo, R., Taylor, S.R., 1976. geochemistry of Eocene calc-alkaline volcanic rocks from the Kastomonu area, northern Turkey. *Contributions to Mineralogy and Petrology* 58, 63–81.
- Renne, P.R., Swisher, C.C., Deino, A.L., Karner, D.B., Owens, T., DePaolo, D.J., 1998. Intercalibration of standards, absolute ages and uncertainties in $^{40}\text{Ar}/^{39}\text{Ar}$ dating. *Chemical Geology* 145, 117–152.
- Roddick, J.C., 1983. High precision intercalibration of ^{40}Ar – ^{39}Ar standards. *Geochimica et Cosmochimica Acta* 47, 887–898.
- Schubert, G., Tackley, P.J., 1995. Mantle dynamics: the strong control of the spinel-perovskite transition at a depth of 660 km. *Journal of Geodynamics* 20, 417–428.
- Şengör, A.M.C., Natal'in, B.A., 1996. Paleotectonics of Asia: fragments of a synthesis. In: Yin, A., Harrison, T.M. (Eds.), *The Tectonic Evolution of Asia*. Cambridge University Press, New York, pp. 486–640.
- Şengör, A.M.C., Natal'in, B.A., Burtman, V.S., 1993. Evolution of the Altaid tectonic collage and Paleozoic crustal growth in Eurasia. *Nature* 364, 299–307.
- Shatkov, G.A., Solovyev, N.S., Shatkova, L.N., Yakobson, L.N., 1980. The principal pattern of the Mongol-PriArgun belt, and chemistry of volcanic rocks. In: Marinov, N.A. (Ed.), *Geology and Mineral Resources of Mongolia*, 1. Nedra Press, Moscow, pp. 35–56.
- Shuvalov, V.F., 1988. The radiological dating of basalts of Tsagaan Tsav formation. *Proceedings of the USSR academy of Sciences. Geological Series*, 10, pp. 68–77.
- Sinton, J.M., Ford, L., Chappell, B., McCulloch, M., 2003. Magma genesis and mantle heterogeneity in the Manus back-arc basin, Papua New Guinea. *Journal of Petrology* 44, 159–195.
- Solovyev, N.S., Shatkov, G.A., Yakobson, L.N., 1977a. PriArgun-Mongolian volcanic belt. *Geology and Geophysics* 3, 20–31.
- Solovyev, N.S., Shatkov, G.A., Yakobson, L.N., 1977b. The Pri-Argun-Mongolian volcanic belt. *Geology and Geophysics* 3, 20–31.
- Steiger, R.H., Jäger, E., 1977. Subcommittee on geochronology: convention on the use of decay constants in geo- and cosmo-chronology. *Earth and Planetary Science Letters* 36, 359–363.
- Stern, R.J., Lin, P.-N., Morris, J.D., Jackson, M.C., Fryer, P., Bloomer, S.H., Ito, E., 1990. Enriched back-arc basin basalts from the northern Mariana Trough: implications for the magmatic evolution of back-arc basins. *Earth and Planetary Science Letters* 100, 210–225.
- Sun, S.S., McDonough, W.F., 1989. Chemical and isotopic systematics of oceanic basalts: implications for mantle composition and processes. In: Saunders, A.D., Norry, M.J. (Eds.), *Magmatism in the Ocean Basins*. Geological Society of London, Special Publications, 42, pp. 313–345.
- Tackley, P.J., 2000. Mantle convection and plate tectonics: toward an integrated physical and chemical theory. *Science* 288, 2002–2007. <http://dx.doi.org/10.1126/science.288.5473.2002>.
- Tackley, P.J., Stevenson, D.J., Glatzmaier, G.A., Schubert, G., 1993. Effects of an endothermic phase transition at 670 km depth in a spherical model of convection in the Earth's mantle. *Nature* 361, 699–704. <http://dx.doi.org/10.1038/361699a0>.
- Taira, A., 2001. Tectonic evolution of the Japanese island arc system. *Annual Review of Earth and Planetary Sciences* 29, 109–134.
- Tauson, L.V., Antipin, V.S., Zakharov, M.N., Zubkov, V.S., 1984a. Geochemistry of Latite of East Far Baikal. *Nauka, Novosibirsk* (214 pp.).
- Tauson, L.V., Antipin, V.S., Zakharov, M.N., Zubkov, V.S., 1984b. *Mesozoic Latite Geochemistry in Trance-Baikal*. Nauka Press, Novosibirsk (214 pp.).
- Taylor, B., Karner, G.D., 1983. On the evolution of marginal basins. *Reviews of Geophysics* 21 (8), 1727–1741.
- Taylor, B., Martinez, F., 2003. Back-arc basin basalt systematics. *Earth and Planetary Science Letters* 210, 481–497.
- Tomurtogoo, O., 1999. *Geological Map of Mongolia with Brief Explanation*.
- Turner, S., Hawkesworth, C., 1998. Using geochemistry to map mantle flow beneath the Lau Basin. *Geology* 26, 1019–1022.
- Van der Voo, R., Spakman, W., Bijwaard, H., 1999. Mesozoic subducted slabs under Siberia. *Nature* 397, 246–249. <http://dx.doi.org/10.1038/16686>.
- Volpe, A.M., Macdougall, J.D., Hawkins, J.W., 1987. Mariana Trough basalts (MTB): trace element and Sr–Nd isotope evidence for mixing between MORB-like and arc-like melts. *Earth and Planetary Science Letters* 82, 241–254.
- Wang, H.Z., Mo, X.X., 1995. An outline of the tectonic evolution of China. *Episodes* 18, 6–16.
- Wang, F., Zhou, X.H., Zhang, L.X., Ying, J.F., Zhang, Y.T., Wu, F.Y., Zhu, R.X., 2006. Late Mesozoic volcanism in the Greater Xing'an Range (NE China): timing and implications for the dynamics setting of NE Asia. *Earth and Planetary Science Letters* 251, 179–198.
- Wang, T., Zheng, Y., Zhang, J., Zeng, L., Donskaya, T., Guo, L., Li, J., 2011. Pattern and kinematic polarity of late Mesozoic extension in continental NE Asia: perspectives from metamorphic core complexes. *Tectonics* 30, TC6007. <http://dx.doi.org/10.1029/2011TC002896>.
- Wang, T., Guo, L., Zheng, Y., Donskaya, T., Gladkochub, D., Zeng, L.S., Li, J.B., Wang, Y.B., Mazukabzov, A., 2012. Timing and processes of late Mesozoic mid-lower-crustal extension in continental NE Asia and implications for the tectonic setting of the destruction of the North China Craton: Mainly constrained by zircon U–Pb ages from metamorphic core complexes. *Lithos* 154, 315–345.
- Windley, B.F., Alexeev, D.V., Xiao, W., Kröner, A., Badarch, G., 2007. Tectonic models for accretion of the Central Asian Orogenic Belt. *Journal of the Geological Society of London* 164, 31–47.
- Wood, D.A., 1980. The application of a Th–Hf–Ta diagram to problems of tectonomagmatic classification and to establishing the nature of crustal contamination of basaltic lavas of the British Tertiary volcanic province. *Earth and Planetary Science Letters* 50, 11–30.
- Wu, F.Y., Yang, J.H., Wilde, S.A., Zhang, X.O., 2005a. Geochronology, petrogenesis and tectonic implications of Jurassic granites in the Liaodong Peninsula, NE China. *Chemical Geology* 221, 127–156.
- Wu, F.Y., Lin, J.Q., Wilde, S.A., Zhang, X.O., Yang, J.H., 2005b. Nature and significance of the Early Cretaceous giant igneous event in eastern China. *Earth and Planetary Science Letters* 233, 103–119.
- Xiao, W.J., Huang, B.C., Han, C.M., Sun, S., Li, J.L., 2010. A review of the western part of the Altai: a key to understanding the architecture of accretionary orogens. *Gondwana Research* 18, 253–273.
- Yanshin, A. L. (Ed.), 1978. *Mesozoic and Cenozoic tectonic map of Mongolian People's Republic*, scale 1: 1500 000. Moscow.
- Yanshin, A. L. (Ed.), 1989. *Geological formations map of Mongolian People's Republic*, scale 1: 1500 000. Moscow.
- Yarmolyuk, V.V., Kovalenko, V.I., Ivanov, V.G., 1995. The Late Mesozoic–Cenozoic Interplate Volcanic Province in Central East Asia: a projection of mantle hot field. *Geotectonics* 5, 41–67.
- Yin, A., 1989. Origin of regional, rooted low-angle normal faults—a mechanical model and its tectonic implications. *Tectonics* 8, 469–482.
- Yin, A., 2010. Cenozoic tectonics of Asia: a preliminary synthesis. *Tectonophysics* 488, 293–325.
- Yin, A., Nie, S., 1996. A Phanerozoic palinspastic reconstruction of China and its neighboring regions. In: Yin, A., Harrison, T.M. (Eds.), *The Tectonic Evolution of China*. Cambridge University Press, Cambridge, pp. 442–485.
- Ying, J.F., et al., 2010a. Geochronological framework of Mesozoic volcanic rocks in the Great Xing'an Range, NE China, and their geodynamic implications. *Journal of Asian Earth Sciences* 39, 786–793 2010a.
- Ying, J.F., Zhou, X.H., Zhang, L.C., Wang, F., 2010b. Geochronological and geochemical investigation of the late Mesozoic volcanic rocks from the Northern Great Xing'an Range and their tectonic implications. *International Journal of Earth Sciences* 39, 786–793.
- Zhang, J.H., Ge, W.C., Wu, F.Y., Wilde, S.A., Yang, J.H., Liu, X.M., 2008. Large-scale Early Cretaceous volcanic events in the northern Great Xing'an Range, Northeastern China. *Lithos* 102, 138–157.
- Zhang, L.C., Zhou, X.H., Ying, J.F., Wang, F., Guo, F., Wan, B., Chen, Z.G., 2008. Geochemistry and Sr–Nd–Pb–Hf isotopes of the Early Cretaceous basaltic rocks in Great Xing'an

- Range, NE China: implication for tectonic setting and characteristics of magmatic sources. *Chemical Geology* 256, 12–23.
- Zhang, J.H., Gao, S., Ge, W.H., Wu, F.W., Yang, J.H., Wilde, S.A., Li, M., 2010. Geochronology of the Mesozoic volcanic rocks in the Great Xing'an Range, northeastern China: implications for subduction-induced delamination. *Chemical Geology* 276, 144–165.
- Zhang, F.Q., Chen, H.L., Yu, X., Dong, C.W., Yang, S.F., Pang, Y.M., Batt, G.E., 2011. Early Cretaceous volcanism in the northern Songliao Basin, NE China, and its geodynamic implication. *Gondwana Research* 19, 163–176.
- Zhang, L., Han, B.-F., Chen, J.-F., Xu, Z., 2012. Sr–Nd isotopic characteristics of the Late Cretaceous Shuangyashan suite: evidence for enriched mantle in Northeast China. *Geol. Mag.* 149 (4), 645–661.
- Zhao, D.-P., Tian, Y., Lei, J.-S., Liu, L., Zheng, S.-H., 2009. Seismic image and origin of the Changbai intraplate volcano in East Asia: role of big mantle wedge above the stagnant Pacific slab. *Physics of the Earth and Planetary Interiors* 173, 197–206.
- Zhao, L., Gao, F.H., Zhang, Y.L., Xu, H.M., Zhang, L.Y., 2013. Zircon U–Pb chronology and its geological implications of Mesozoic volcanic rocks from the Hailaer basin. *Acta Petrologica Sinica* 29, 864–874 (in Chinese with English abstract).
- Zhou, X., Sun, T., Shen, W., Shu, L., Niu, Y., 2006. Petrogenesis of Mesozoic granitoids and volcanic rocks in South China: a response to tectonic evolution. *Episode* 29, 26–32.
- Zindler, A., Hart, S., 1986. Annual review of earth and planetary sciences. *Chemical Geodynamics* 14, 493–571.
- Zonenshain, L.P., Kuzmin, M.I., Natapov, L.M., 1990. *Geology of the USSR: a plate-tectonic synthesis*. AGU Geodynamic Series 21, 250.